AGU PUBLICATIONS

Global Biogeochemical Cycles

RESEARCH ARTICLE

10.1002/2016GB005411

Key Points:

- We report the first ever measurements of Hg stable isotopes in polar firn and ice cores
- Hg isotope ratios in Arctic firn and ice differ from that of snow impacted by atmospheric Hg depletion events
- Changes in Hg isotope ratios in High Arctic firn appear to track the evolving composition of global Hg emissions

Supporting Information:

- Supporting Information S1

Correspondence to:
C. M. Zdanowicz,
christian.zdanowicz@geo.uu.se

Citation:
Zdanowicz, C. M., E. M. Krümmel, A. J. Poulain, E. Yumvihoze, J. Chen, M. Štrok, M. Scheer, and H. Hintelmann (2016), Historical variations of mercury stable isotope ratios in Arctic glacier firn and ice cores, *Global Biogeochem. Cycles*, *30*, doi:10.1002/2016GB005411.

Received 5 MAR 2016
Accepted 16 AUG 2016
Accepted article online 23 AUG 2016

Historical variations of mercury stable isotope ratios in Arctic glacier firn and ice cores

C. M. Zdanowicz[1], E. M. Krümmel[2], A. J. Poulain[3], E. Yumvihoze[3], J. Chen[4], M. Štrok[5,6], M. Scheer[7], and H. Hintelmann[6]

[1]Department of Earth Sciences, Uppsala University, Uppsala, Sweden, [2]Inuit Circumpolar Council of Canada, Ottawa, Ontario, Canada, [3]Department of Biology, University of Ottawa, Ottawa, Ontario, Canada, [4]State Key Laboratory of Environmental Geochemistry, Chinese Academy of Sciences, Guyiang, China, [5]Jožef Stefan Institute, Ljubljana, Slovenia, [6]Department of Chemistry, Trent University, Peterborough, Ontario, Canada, [7]Scheer Software Solutions, Barry's Bay, Ontario, Canada

Abstract The concentration and isotopic composition of mercury (Hg) were determined in glacier core samples from Canadian Arctic ice caps dating from preindustrial to recent time (early 21st century). Mean Hg levels increased from ≤ 0.2 ng L^{-1} in preindustrial time to ~0.8–1.2 ng L^{-1} in the modern industrial era (last ~200 years). Hg accumulated on Arctic ice caps has Δ^{199}Hg and Δ^{201}Hg that are higher (~ −1 to 2.9‰) than previously reported for Arctic snow impacted by atmospheric Hg depletion events (mostly < -1‰), suggesting that these events contribute little to Hg accumulation on ice caps. The range of δ^{202}Hg, Δ^{199}Hg, and Δ^{201}Hg in glacier cores overlaps with that of Arctic $Hg^0_{(g)}$ and of seawater in Baffin Bay and also with that of midlatitude precipitation and industrial Hg sources, including coal and Hg ores. A core from Agassiz ice cap (80.7°N) shows a ~ +1‰ shift in δ^{202}Hg over the nineteenth to twentieth centuries that could reflect changes in the isotopic composition of the atmospheric Hg pool in the High Arctic in response to growing industrial emissions at lower latitudes. This study is the first ever to report on historical variations of Hg stable isotope ratios in Arctic ice cores. Results could help constrain future modeling efforts of the global Hg biogeochemical cycle and the atmosphere's response to changing Hg emissions, past and future.

1. Introduction

Mercury (Hg) is a global contaminant that poses a threat to humans and ecosystems worldwide [*Driscoll et al.*, 2013]. Growing concerns about Hg pollution led the international community to adopt, in 2013, the Minamata Convention on Mercury, a global treaty to protect human health and the environment from the adverse effects of Hg [*United Nations Environment Programme*, 2013]. Owing in part to the volatility of its elemental form ($Hg^0_{(g)}$), Hg can be transported and dispersed globally via the atmosphere or oceans and contaminate high-latitude environments far away from anthropogenic emission point sources [*Fitzgerald et al.*, 1998]. Over the past decade, much research has been devoted to identify possible pathways and processes by which Hg enters Arctic ecosystems [*Arctic Monitoring and Assessment Programme*, 2011]. While progress has been made, the actual geographical extent and magnitude of past and present atmospheric Hg pollution in the Arctic remains uncertain [e.g., *Goodsite et al.*, 2013].

Recent developments in the determination of stable Hg isotope ratios in various environmental media have opened new and promising avenues of research to identify the source(s) and processes involved in the transfer of Hg into the environment (see *Blum et al.* [2014] for a recent review). Hg has seven different stable isotopes (mass numbers 196, 198, 199, 200, 201, 202, and 204) which can be subject to both mass-dependent and mass-independent fractionation (MDF and MIF, respectively) during various physicochemical transformations, biotic or abiotic. The isotopic signatures of Hg in different media (soil, precipitation, air, and organic tissues) that are inherited during the cycling of Hg can therefore be used as tracers to identify the source(s) and processes involved and also help constrain the development of global models of Hg cycling in the environment [e.g., *Yin et al.*, 2010; *Sonke*, 2011].

In this study, we determined the concentration and stable isotope composition of Hg in glacier firn and ice cores in order to investigate possible sources and trends of atmospheric Hg deposition in the Arctic environment over past decades, centuries, and millennia. We took advantage of the recent development of preconcentration techniques for the determination of Hg isotope ratios in water samples [*Chen et al.*, 2010; *Štrok et al.*, 2014] and applied these to archived glacier firn and ice cores collected at multiple sites across the Canadian Arctic

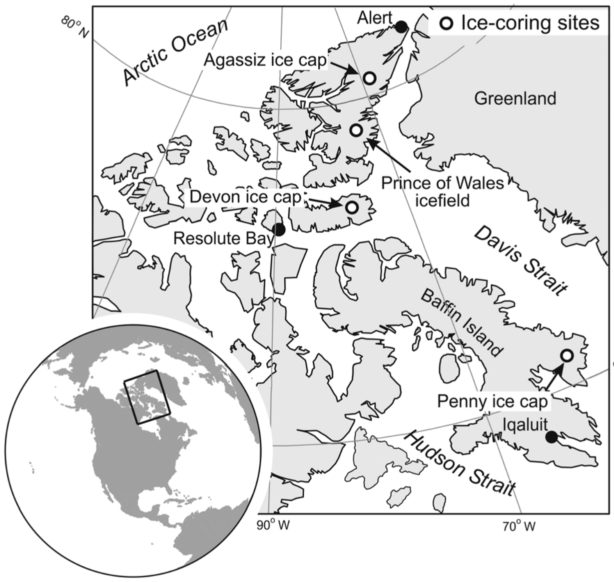

Figure 1. Location map of the eastern part of the Canadian Arctic Archipelago.

Archipelago. These samples range in age from recent decades to more than ten millennia. Given the logistical difficulty and high cost of obtaining firn or ice cores from remote Arctic locations, we sought to establish if variations in the isotope composition of Hg could first be identified in archived core material already on hand. Specifically, the main questions we sought to answer were the following: (1) Is there a discernable difference between the stable isotope composition of Hg accumulated in ancient (preindustrial) ice and more recent (industrial era) firn layers? (2) How has the stable isotope composition of Hg in firn varied over the past 200 years (since the onset of the Industrial Revolution)? (3) Does the range and variability of Hg stable isotope ratios in Arctic firn and ice layers provide some indications on possible dominant Hg sources in the recent and more distant past and on the physicochemical processes that control these ratios?

2. Study Area

Our sample material consists of segments of glacier firn or ice cores recovered from four ice caps located between latitudes 67.2 and 80.7°N in the eastern part of the Canadian Arctic Archipelago: Agassiz ice cap and the Prince of Wales icefield (Ellesmere Island), Devon ice cap (Devon Island), and Penny ice cap (Baffin Island) (Figure 1). These ice caps range in size from ~6300 km^2 (Penny ice cap) to ~19,325 km^2 (Prince of Wales icefield), and some reach elevations of nearly 2000 m above sea level (asl). All these ice caps are affected by air masses and precipitation advected from the Baffin Bay sector, and the northernmost ones in the Queen Elizabeth Islands are also under the influence of air flow from the Arctic Ocean. Compared to the interior regions of the Greenland ice sheet, the smaller Canadian Arctic ice caps are more exposed to marine influences, as aerosol transport distances from coastal areas are typically of a few tens of kilometers.

Direct atmospheric observations, modeling, and ice core data demonstrate that there is direct transport of polluted air into the Canadian Arctic from latitudes down to 40°N [*Goto-Azuma and Koerner*, 2001; *Durnford et al.*, 2010; *Kuhn et al.*, 2010; *Zdanowicz et al.*, 2013]. Thus, as will be discussed later, atmospheric Hg deposited on ice caps in this region may originate from both proximal (marine) and distant (continental) sources, including anthropogenic pollution emissions. Present-day mean atmospheric Hg fluxes (i.e., net deposition rates) on Canadian Arctic ice caps have been estimated from snow and ice core measurements and range between 0.07 and 0.16 $\mu g\,m^{-2}\,a^{-1}$ (Table 1) [*Zdanowicz et al.*, 2013, 2015; *Zheng*, 2014; *Gamberg et al.*, 2015].

3. Materials and Methods

3.1. Firn and Ice Cores

All cores used in this study were recovered between 1994 and 2005 by the Geological Survey of Canada (Table 1). Most of these cores were drilled using an electromechanical ice drill with steel cutters and a stainless steel sonde with an inner diameter of 8.4 cm. The cores were kept in freezer storage in Ottawa ($-25 < T < -15$°C), packed in high-density polyethylene layflat bags inside opaque, insulated boxes. Some of the cores had been subsampled for prior analyses, and the remaining segments were quarter- or half-diameter cores kept as reference material. The volume of usable core material was limited by the need to remove outer core layers to eliminate possible contamination introduced during or after drilling.

Table 1. Details of Canadian Arctic Firn and Ice Cores Used in This Study

Site	Core(s)	Year Drilled	Latitude (°N)	Longitude (°W)	Elevation (m)	MAST[a] (°C)	$\dot{A}$[b] (m ice a^{-1})	MF[c] (%)	THg Flux[d] ($\mu g\ m^{-2}\ a^{-1}$)	Age Model Used[e]
Agassiz ice cap	AG93.2	1993	80.7	73.1	1860	−24.5	0.10 ± 0.02			GICC05
	AG94.1	1994	80.7	72.8	1670	−21.9	0.18 ± 0.04	~40	0.07 ± 0.02	A77ZT
Prince of Wales icefield	PW05.1	2005	78.4	80.4	1630	−20.9	0.30 ± 0.06	~25	>0.09	TIMECM3
Devon ice cap	DV99.1	1999	75.3	81.6	1903	−23	0.13 ± 0.03	~15	~0.16	TIM3.D99
	PN95.4	1995	67.3	65.8	1860	−15.9	0.40 ± 0.08		0.11 ± 0.05	TIMSPEC2.954
Penny ice cap	PN96.2	1996	67.3	65.2	1810	−14.9	0.19 ± 0.04	>70	*unknown*	TIM2.962

[a]MAST: Present-day mean annual surface air temperature at the coring sites.
[b]$\dot{A}$: Present-day mean annual ice accumulation rate at the coring sites.
[c]MF: Present-day (post-1985) mean volumetric percentage of the annual accumulation at each coring site which results from in situ refreezing of surface meltwater [*Fisher et al.*, 2012].
[d]Estimates of present-day THg net depositional fluxes are taken from *Gamberg et al.* [2015, and references therein]. Note that figures for Prince of Wales icefield and Devon ice cap are based on limited data. These estimates assume a plausible interannual variability in $\dot{A}$ of ± 20%.
[e]The AG94.1 core was drilled at the same site as an earlier core (AG77), and the depth-age model used was the same as that developed from this earlier core [*Fisher and Koerner*, 1995]. Development of the age model for the DV99.1 core was based on electrical conductivity measurements and correlation with that of another, independently dated core (DV98.3) [*Kinnard et al.*, 2006]. For the other cores, details of the age models can be found in the following publications: AG93.2, *Vinther et al.* [2008]; AG94.1, *Fisher et al.* [1995]; PW05.1, *Kinnard et al.* [2008]; PN95.4 and PN96.2, *Fisher et al.* [1998] and *Okuyama et al.* [2003].

Furthermore, total Hg concentrations in Arctic glacier ice and snow, hereafter denoted [THg], are typically very low (≤3 ng L^{-1}) [*Gamberg et al.*, 2015], and it was therefore necessary to melt and combine multiple sections of cores to obtain a sufficient mass of Hg for accurate determination of isotopic ratios after preconcentration (see section 3.4 below).

The age structure of firn and ice in polar ice caps and the pore close-off depth are determined largely by the net snow accumulation rate $(\dot{A})$. Depth-age models have been developed for Canadian Arctic ice caps with an ice flow model using estimates of $\dot{A}$ and constrained by reference horizons such as the chemical signature of historically dated volcanic eruptions or distinctive features in the oxygen isotope profiles ($\delta^{18}O$) that can be correlated with similar features in well-dated Greenland cores [*Fisher et al.*, 1995, 1998; *Okuyama et al.*, 2003; *Kinnard et al.*, 2006, 2008; *Vinther et al.*, 2008]. The estimated age span of the various core samples used in the present study is shown in Figure 2.

Owing to dynamic thinning of glacier ice layers, age-depth relationships are nonlinear, and the time span represented by a ~1 m long core segment increases from a few years near the surface to millennia at depths > 100 m. On three out of four ice caps covered in this study, the estimated age at the firn-ice transition depth exceeds 200 years. Therefore, snow that accumulated at most of the coring sites during the modern industrial era is preserved in the form of firn and has not yet turned into glacier ice. The implications of this for Hg analyses are discussed below. In this study, all glacier ice core samples (density ≈ 0.92 kg m^{-3}) are referred to as “preindustrial,” and all firn cores (density < 0.92 kg m^{-3}) are considered to be of “industrial era” age. Estimated ages for preindustrial cores range from ~925 to >10,000 years b.p. (before present, where 2010 A.D. is used as the reference year). Large dating uncertainties up to ± 500 years in deep ice core segments (below ~100 m) do not allow for a more precise discrimination. For the firn cores, the estimated age span is from the early 19th century (~1808) to the early 21st century (~2004).

3.2. Core Subsampling Procedures

The various firn and ice cores were kept in cold storage for 5 to 18 years (Table 1). Due to varying storage conditions over these long intervals, some archived core segments showed frost accretion on their outer surfaces. A few also showed indications of partial melt (e.g., ice glands at the surface). These features formed when temperature in the freezer rose during

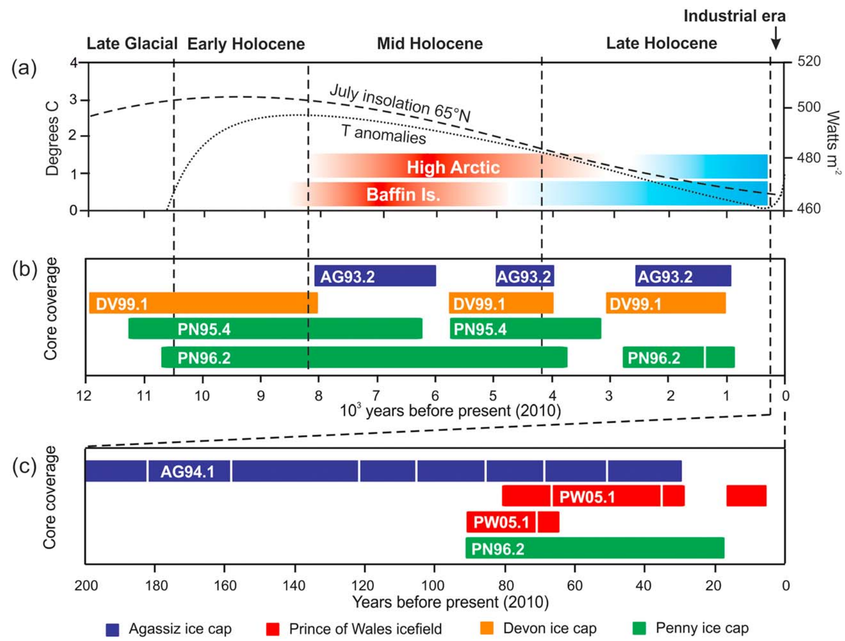

Figure 2. (a) Changing climate conditions at northern high latitudes over the past 12,000 years. Holocene subdivisions (early, middle, and late) are as proposed by *Walker et al*. [2012]. The two curves show orbitally induced changes in mid-summer insolation at 65°N [*Berger*, 1992], and estimated July air temperature anomalies over Greenland relative to the late nineteenth century, based on ice core $\delta^{18}O$ paleothermometry [*Vinther et al*., 2008]. Colored bars indicate the approximate timing of maximum warmth during the early to middle Holocene (red) and transition to late Holocene neoglaciation (blue) in the High Arctic and the Baffin Island region, based on multiproxy reconstructions [*Briner et al*., 2016]. (b and c) The estimated accumulation time intervals represented by the Canadian Arctic firn and ice core segments analyzed for Hg isotope ratios as part of this study. The cores are identified in Table 1. Note that core PW05.1 has two parallel, overlapping sets of samples.

maintenance defrosting of the ventilation system or occasionally due to compressor malfunction. Superficial melt features and/or accreted frost layers were first removed by scraping prior to further decontamination.

The firn and ice core segments selected for analysis underwent further processing steps to remove outer layers that could have been contaminated with Hg during drilling, previous subsampling, manipulations, or storage. The outer layers of most firn cores (~3 to 5 mm) were removed inside a cold room at the Geological Survey of Canada's ice core laboratory. Previous experience with trace metal analyses showed that this is usually sufficient to remove outer contamination [*Zheng et al*., 2006]. The removal of the outer firn layers and ends of core sections was done using a titanium chisel and/or a stainless steel band saw that had been precleaned by cutting pure ice blocks (frozen Milli-Q water). How much was removed from each core segment depended on the available volume and texture: less material was removed from cores with a higher density and compactness. An exception was made for three sections of a shallow (7.73 m long) snow/firn core recovered in April 2005 from the Prince of Wales icefield using a fiberglass corer. This core had never been handled since collected and had remained packed in its original bag. Being the "freshest" archived core material available to us, determining its [THg] and Hg isotopic ratios was regarded as a priority in order to compare results with those of older, deeper firn layers. However, the density of firn layers in the core was relatively low (290–630 kg m^{-3}, averaging 470 kg m^{-3}), and it was feared that scraping off the outer layers might leave an insufficient volume of meltwater for analysis. Hence, the core sections were melted without any decontamination. Analysis subsequently showed that [THg] in the shallow core samples are statistically undistinguishable from those measured in the center part of precleaned firn core sections of comparable age or slightly older, taken at the same site (see section 4.1).

For the precleaned cores, both the ice shavings (outer layers) and the remaining inner-core segments were sealed inside Hg-free Teflon bags and kept frozen until analyzed. For glacier ice cores (density ≈ 920 kg m^{-3}), the decontamination steps were carried out inside a Hg-free, Class 100 clean room at the Laboratory for the Analysis of Natural and Synthetic Environmental Toxins (LANSET) at the University of Ottawa. There core segments were partially thawed at normal room temperature (20°C) inside their bags, until ~5 mm of ice had melted from the outer layers. Once the ice was partially thawed, the bags containing the cores were cut open, the meltwater was collected separately, and the remaining ice pieces were rinsed with double-distilled water. They were then placed inside Hg-free, sealable Teflon bags, and immediately frozen again until analysis.

3.3. Total Mercury and Methylmercury Analyses

Measurements of [THg] in firn and ice cores were performed at LANSET, University of Ottawa, and at the Water Quality Center of Trent University, Ontario, where the Hg isotope determinations were also carried out (see section 3.4 below). In this paper, we use results from Trent University to quantify temporal [THg] variations in firn and glacier ice, where feasible. Over 100 discrete [THg] measurements were performed in order to establish the number of subsamples needed to obtain a sufficient mass of THg for reliable Hg isotope ratio determination. Analyses at the University of Ottawa were done mainly for the purpose of controlling the efficacy of the core decontamination procedure, and these included measurements of [THg] in meltwater from the outer layers of ice core segments. In addition, a subset of decontaminated, inner-core samples were analyzed in both Trent and Ottawa to compare results. Owing to limitations in the volume of core material available, the samples used for this comparison exercise could not be matched exactly, although they came from core segments of comparable depth and age. A summary of all THg analyses performed is provided in Table S1 in the supporting information.

All determinations of [THg] at the University of Ottawa and at Trent University were performed by cold vapor-atomic fluorescence spectrometry (CV-AFS), following U.S. Environmental Protection Agency method 1631E [*U.S. Environmental Protection Agency*, 2002], which involves an initial oxidation step of Hg species to Hg^{II} using BrCl. Total Hg, as defined in this method, therefore comprises all BrCl-oxidizable Hg species present in the melted firn/ice samples. There are presently no detailed Hg speciation data on ancient glacier firn and ice, but studies on modern Arctic snow suggest that Hg^0 only accounts for a very small percentage of THg [*Poulain et al*., 2004]. Furthermore, evasion of gaseous Hg from porous firn samples, or of dissolved $Hg^0_{(g)}$ from melted firn or ice samples, probably leaves little Hg^0 in these samples, such that the THg determined by CV-AFS most likely represents the sum of other, nonvolatile but BrCl-oxidizable species.

The method detection limits (MDL) for the CV-AFS analyses were estimated by the standard deviation of three to four replicate measurements of reagent blanks per sample batch (see Table S2 for details). For the University of Ottawa, MDL ranged from 0.01 to 0.03 ng L^{-1}, with a median of 0.02 ng L^{-1} ($n = 24$). For Trent University, MDL varied between 0.01 and 0.33 ng L^{-1}, with a median of 0.05 ng L^{-1} ($n = 104$). However, low [THg] which are reliably determined to exceed MDL are not necessarily quantifiable with a high level of confidence. We therefore used the minimum level of quantitation (ML) as a measure of the lowest detectable [THg] that can be reliably quantified, with ML = 3.18 × MDL, following *U.S. Environmental Protection Agency* [2002]. For the University of Ottawa, the median ML for [THg] was 0.05 ng L^{-1}, and for Trent University, it was 0.20 ng L^{-1}. For each batch of samples analyzed, combined standard uncertainties (u_c) on [THg] were estimated as the quadratic sum of the standard uncertainty of the calibration curves and the standard deviation of replicate analyses of samples or standards. For analyses performed at the University of Ottawa, u_c ranged from 0.06 to 0.60 ng L^{-1}, while at Trent University it ranged from 0.05 to 0.89 ng L^{-1}. For the range of [THg] found in decontaminated firn and ice cores (<4 ng L^{-1}; see below), u_c averaged 0.20 ng L^{-1} at both laboratories.

Methylmercury (MeHg; monomethyl + dimethyl Hg) was also determined in a few selected firn and ice core samples in order to estimate the relative contribution of these particular forms of organic Hg to total accumulation in firn and ice. The analyses were performed at LANSET, University of Ottawa, by capillary gas chromatography coupled with atomic fluorescence spectrometry following a preconcentration step [*Cai et al*., 1996]. The estimated MDL for these measurements was 0.02 ng L^{-1}, and the 2σ uncertainty was ~ ± 15% of [MeHg]. The corresponding ML was 0.06 ng L^{-1}.

3.4. Stable Hg Isotope Ratios

Because of the low [THg] measured in Arctic glacier firn and ice (typically, a few ng L^{-1} or less), the Hg in the melted firn and ice core samples first had to be preconcentrated prior to isotopic ratio determination. Melted core sample volumes ranging from ~2 to 20 L were processed in order to obtain a sufficient mass of Hg. To achieve this, two variants of the same preconcentration method were used. Three ice core samples from Penny ice cap (PN96.2 core) were preconcentrated following the chromatographic protocol developed by *Chen et al*. [2010], while for the remainder of the firn and ice cores, a variant of the same protocol, optimized by *Štrok et al*. [2014] for large-volume samples, was used. The final volumes of concentrated Hg solution obtained after elution were on the order of 3–5 mL, corresponding to preconcentration factors of up to 400.

In their study, *Štrok et al*. [2014] estimated the recovery of Hg by the preconcentration protocol to be 94–100% for sample volumes up to 10 L, without any significant isotopic fractionation of Hg being induced. In our study, recoveries were estimated by comparing the total initial mass $\left(m^i_{\mathrm{THg}}\right)$ of THg measured in the separate ice core segments with that in the combined sample obtained after preconcentration $\left(m^f_{\mathrm{THg}}\right)$. For two of the first samples analyzed in the study (from the PN96.2 core), m^f_{THg} was not measured, and recovery could therefore not be estimated in these samples. For all other samples, the differences between m^i_{THg} and m^f_{THg} were ranked with zeta scores, as is commonly done in interlaboratory comparisons for proficiency testing, following

$$\mathrm{zeta} = \frac{\left|m^f_{\mathrm{THg}} - m^i_{\mathrm{THg}}\right|}{\overline{u_c}} \tag{1}$$

where $\overline{u_c}$ is the quadratic sum of standard analytical uncertainties on both m^i_{THg} and m^f_{THg}. A zeta score ≤ 2 is usually considered satisfactory, i.e., results are deemed identical within analytical uncertainties. The estimated Hg recoveries for our samples after preconcentration ranged from as low as 51.4% to as high as 198.1%, but when analytical uncertainties are accounted for, only four samples gave zeta scores > 2 (Table S3). These came from the AG94.1 core (one sample) and the PW05.1 core (three samples). In three of the samples with zeta scores > 2, m^f_{THg} was ~30–50% less than m^i_{THg}, while in one sample it exceeded m^i_{THg} by ~29%. However, in terms of their Hg isotopic composition, these samples did not differ markedly from others in the same cores with Hg recoveries equal or close to 100%, and none stood out clearly as outliers (see section 4.1). One sample that did appear to be an outlier was from core AG93.2. The estimated recovery for that sample was 198%, but the zeta score was 0. Given these uncertainties, we opted not to exclude those results with high zeta scores, because in doing so we might wrongly reject valid data. However, we clearly identified these samples in our results.

All Hg isotope ratio determinations in this study were performed on a Neptune multicollector inductively coupled mass spectrometer (Thermo-Fisher, Germany) at Trent University. All reagents (HCl, HNO_3, BrCl, L-cysteine, $NH_2OH{\cdot}HCl$, and $SnCl_2$) used in the preparation of samples were analytical grade or prepared under Hg-free condition. All vessels were made of glass or Teflon and were cleaned with 1% BrCl and/or 50% HNO_3 and rinsed with distilled H_2O before their use. The University of Michigan's (UM)-Almadén Hg standard was used as a reference material and was measured regularly to control the quality of isotopic measurements (Table S4).

For the Hg isotope measurements, the preconcentrated Hg sample solutions were introduced into the plasma by a continuous flow cold vapor generation system equipped with an additional Nafion drier tube [*Chen et al*., 2010]. The $SnCl_2$ reducing agent was mixed online with the Hg solution to generate volatile elemental Hg. A Tl aerosol produced from an Apex desolvation system was simultaneously introduced into the plasma for mass bias correction. The Faraday cups were positioned to measure five Hg isotopes (^{198}Hg, ^{199}Hg, ^{200}Hg, ^{201}Hg, and ^{202}Hg) and two Tl isotopes (^{203}Tl and ^{205}Tl). The instrumental mass bias was corrected using the modified empirical external normalization method [*Chen et al*., 2010]. Following a widely accepted usage, the MDF of Hg isotopes was expressed in delta notation (δ^xHg, in ‰) as defined by the equation

$$^{x}\mathrm{Hg} = \left\{ \frac{\left(^{x}\mathrm{Hg}/^{198}\mathrm{Hg}\right)_{\mathrm{sample}}}{\left(^{x}\mathrm{Hg}/^{198}\mathrm{Hg}\right)_{\mathrm{standard}}} - 1 \right\} \times 1000 \tag{2}$$

Table 2. [THg] in Outer and Inner Layers of Firn and Ice Core Samples[a]

Outer Core (University of Ottawa)		Inner Core (University of Ottawa)		Inner Core (Trent University)	
Segment #	[THg] (ng L^{-1})	Segment #	[THg] (ng L^{-1})	Segment #	[THg] (ng L^{-1})
Agassiz 1993.2 (Estimated Core Ages: 1200 to 7660 Years b.p.)					
78	5.11	78	0.58	75 + 78	0.43
94	3.56	94	0.12	93 + 94 + 95	0.02
101 + 102	2.77	101 + 102	0.12	101 + 102	0.12
118	2.10	118	0.41	117 + 118	0.05
124	3.68	124	0.12	124 + 125	0.04
138	4.58	138	0.36	135 + 138	0.10
142 + 143	50.01	142 + 143	0.17	142 + 143 + 144	0.09
Agassiz 1994.1 (Estimated Core Ages: 1808 to 1980 A.D.)					
4 + 7	3.76			4 + 7	0.94
8 + 10	2.28			9 + 10	0.83
11 + 13	1.59			11 + 13	1.08
14 + 16	1.94			15 + 16	0.99
17 + 21	2.19			20 + 21	0.44
34 + 35	0.94			33 + 34	0.52
36 + 37	1.37			36 + 37	0.70
37 + 39	1.42			37 + 39	0.66
40 + 41	1.26			39 + 41	0.56
42 + 43	1.20			41 + 42	0.96
43 + 45	1.41			43 + 44 + 45	0.88

[a]The numbered core segments (or combination of segments) compared in this table are of approximate matching depths and ages. The [THg] values reported are either single measurements on composite samples or mean values for multiple core segments.

where $x = 199$, 200, 201, 202, and "standard" represents the international standard NIST SRM 3133 Hg solution. The MIF of Hg isotopes (both odd and even) was defined by the deviation from the theoretically predicted MDF and was expressed as (in ‰)

$$\Delta^{199}\text{Hg} = \delta^{199}\text{Hg} - \left(0.252 \times \delta^{202}\text{Hg}\right) \tag{3}$$

$$\Delta^{200}\text{Hg} = \delta^{200}\text{Hg} - \left(0.502 \times \delta^{202}\text{Hg}\right) \tag{4}$$

$$\Delta^{201}\text{Hg} = \delta^{201}\text{Hg} - \left(0.752 \times \delta^{202}\text{Hg}\right) \tag{5}$$

In this paper, we use δ^{202}Hg as shorthand to quantify MDF for all Hg isotopes, and Δ^{200}Hg and Δ^{199}Hg or Δ^{201}Hg to quantify MIF of even- and odd-numbered Hg isotopes, respectively.

Repeated measurements of the UM-Almadén reference material (Table S4) gave mean values of -0.20 ± 0.10‰, -0.32 ± 0.10‰, -0.42 ± 0.12‰, and -0.57 ± 0.12‰ for δ^{199}Hg, δ^{200}Hg, δ^{201}Hg, and δ^{202}Hg, respectively, and -0.06 ± 0.09‰, -0.03 ± 0.08‰, and -0.01 ± 0.09‰ for Δ^{199}Hg, Δ^{200}Hg, and Δ^{201}Hg, respectively ($\pm 1\sigma$, $n = 23$). These results are in close agreement with those from previous studies [*Bergquist and Blum*, 2007; *Blum and Bergquist*, 2007; *Chen et al.*, 2010, 2012; *Jiskra et al.*, 2012]. Because the small volume of the preconcentrated samples did not allow for replicate measurements, the external reproducibility of the method for all samples was calculated instead as twice the external standard deviation ($\pm 2\sigma$) of replicate analyses of the UM-Almadén standard: ±0.20‰ for δ^{199}Hg and δ^{200}Hg, ±0.24‰ for δ^{201}Hg and δ^{202}Hg, and ±0.18‰, ±0.16‰, and ±0.18‰ for Δ^{199}Hg, Δ^{200}Hg, and Δ^{201}Hg, respectively. An estimate of the reproducibility of results using actual samples can be obtained from *Chen et al.* [2012], who performed duplicate or triplicate determinations of Hg isotopic ratios on preconcentrated rain and snow samples, many of which had [THg] comparable to those in our own firn and ice samples (0.35 to 4 ng L^{-1}). The measurements by *Chen et al.* [2012, Table 1] were performed on the same mass spectrometer and under the same operating conditions as our own samples. The mean and median uncertainties calculated from *Chen et al.*'s [2012] samples that had [THg] < 4 ng L^{-1}, as well as for all samples, were all lower than the uncertainties we report in this paper based on replicate analyses of the UM-Almadén standard.

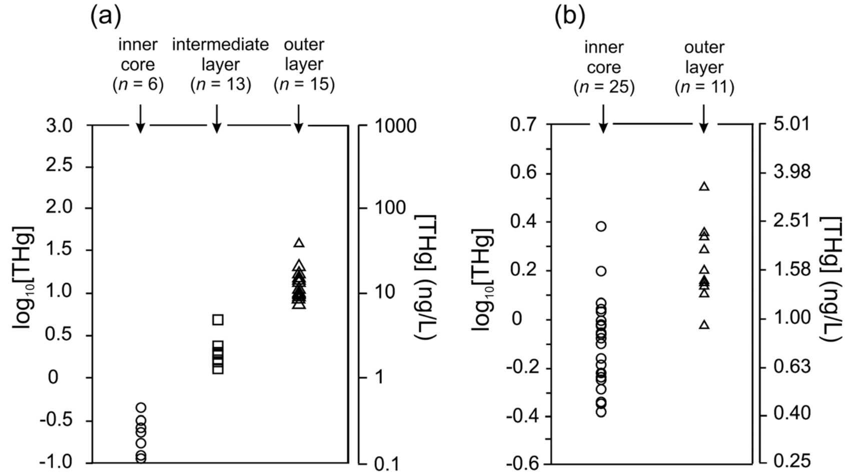

Figure 3. [THg] measured in different layers of firn and ice cores from the Canadian Arctic: (a) Penny ice cap PN95.4 core (preindustrial age) and (b) Agassiz ice cap AG94.1 firn core (industrial age). For each core, samples from different layers cover the same depth range, although there is no one-to-one correspondence between samples. The "intermediate layer" in core PN95.4 is from core segments on which the outermost layer had been previously cut and sampled for the determination of oxygen isotope ratios as part of an earlier study. Data symbols representing individual measurements are approximately equal in size, or larger, than their corresponding 2σ error bars.

Detailed results of all THg analyses and Hg isotope ratio determinations on firn and ice core samples performed in this study are provided in Tables S5–S7. The main findings, including results of the MeHg analyses, are summarized in the following sections.

4. Results and Discussion

4.1. Effects of Core Storage and Handling on Hg Measurements

Analyzing trace-level contaminants in polar snow, firn, or ice is challenging, and special clean techniques have been developed to handle such sample material [e.g., *Zheng et al.*, 2006]. Analyzing [THg] is more challenging still, because even in a particle-free clean air laboratory environment, Hg can be deposited onto frozen surfaces from the gas phase [*Bartels-Rausch et al.*, 2008] or can evade samples by photoreduction when exposed to light [*Zheng et al.*, 2014]. Working with archived core samples that have been kept in storage for years to decades, as was done in this study, introduces additional uncertainties, because the effect of long-term storage on Hg preservation in firn or ice has never been quantified.

During sample preparation, we sought to eliminate as much external Hg contamination as possible. As a check on results, we compared [THg] measured in outer and inner layers of selected segments from cores PN95.4 (preindustrial age) and AG94.1 (industrial era) (Table 2 and Figure 3).

This comparison indicates that (1) meltwater from the outer layers of preindustrial ice cores have [THg] that are greater than inner-core samples by at least 1 order of magnitude or sometimes 2 or more; (2) the [THg] in outer-core shavings from firn cores of the industrial era are comparable to or lower than that in the outer layers of preindustrial ice cores; and (3) the [THg] in firn cores of the industrial era are on average higher than those in preindustrial ice cores.

The maximum [THg] in all inner-core samples was 3.88 ng L^{-1} (PW05.1 core). The lowest [THg] were $<$ 0.10 ng L^{-1}, and these were mostly found in the inner layers of preindustrial ice core samples. In contrast, 60% of all outer-core layers, firn or ice, had much higher [THg], with a maximum value of 128.84 ng L^{-1} (PW05.1 core). The higher [THg] values found in the outer layers of ice cores, compared to firn cores, suggest that drilling through ice resulted in greater exterior contamination by trace metals (including Hg), presumably because porous firn opposes less mechanical resistance than ice to the drill sonde and cutters. In addition, most of the ice cores used in this study had been handled and subsampled on multiple occasions (for various types of analyses) since they were recovered, while the High Arctic firn cores (AG94.1 and PW05.1) had seen very limited handling.

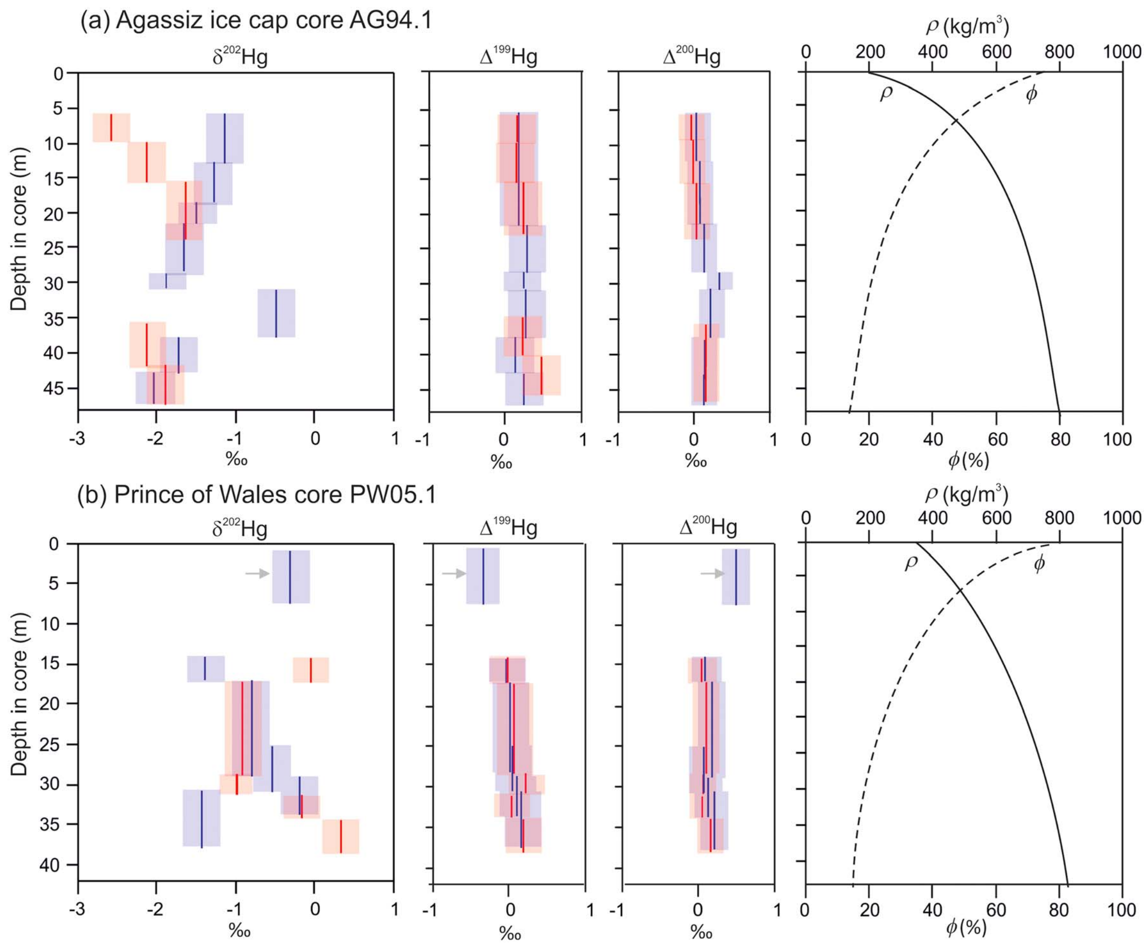

Figure 4. Stable Hg isotope composition of outer-core scrapings (red lines) and inner-core samples (blue lines) in firn cores from (a) Agassiz ice cap (core AG94.1) and (b) Prince of Wales icefield (core PW05.1). The height of each line corresponds to the depth range covered by samples, while the width of the shaded rectangles denote the analytical error (±2σ). The values marked with an arrow in Figure 4b are weighted averages of four samples taken from a shallow snow core. Also shown are mean firn density (ρ) and porosity (φ) profiles at the AG94.1 and PW05.1 coring sites.

The "true" [THg] in the innermost part of the cores can of course not be known a priori, but in view of the results presented above, we consider it likely that we removed most if not all of the external Hg contamination on the core samples. There remains, however, the possibility of Hg losses during long-term core storage or sample preparation, either by outgassing and/or photoreduction of Hg^{II} to $Hg^0_{(g)}$ resulting from exposure to artificial light. *Zheng et al.* [2014] reported a mean [THg] reduction of 17% in snow samples from Agassiz ice cap after 1 year of dark storage at −18°C, although how Hg was lost from the snow in the absence of light has not been established. Since no long-term studies of THg preservation have ever been conducted on firn and ice cores, the magnitude of THg losses from the innermost parts of our core samples during storage cannot be quantified. In the absence of such data, we consider the [THg] values reported here as likely to be minimum values, and we interpret these data accordingly.

The AG94.1 and PW05.1 firn cores provided a sufficient volume of outer-core surface scrapings for Hg isotope ratio determinations, which allowed us to contrast the Hg isotope composition of the inner and outer layers over comparable depth intervals (Figure 4). Down-core patterns of δ^{202}Hg differ considerably, albeit in a nonsystematic way, between inner and outer layers, while Δ^{200}Hg and Δ^{201}Hg patterns are essentially identical, showing little variability. Some outer-core variations in δ^{202}Hg could conceivably result from MDF accompanying reduction of Hg^{II} to Hg^0 during core storage [*Bergquist and Blum*, 2007], or they might reflect contamination by Hg with different δ^{202}Hg than that found in the inner parts of the cores. Our data do not allow us to confidently discriminate between these (or other, undetermined) effects. However, the fact that δ^{202}Hg patterns in the inner cores differ markedly from those in the outer cores suggests that the central part of the

Table 3. Summary of [THg] and Hg Isotopic Composition of Arctic Firn and Ice Cores Analyzed in This Study[a]

	Depth (m)		Age[b] (Years b.p.)		Age[b] (Years A.D.)		[THg][c] (ng L^{-1})		Hg Isotope Composition (‰)						
Core	From	To	From	To	From	To	Range	Mean (n)	δ^{199}Hg	δ^{200}Hg	δ^{201}Hg	δ^{202}Hg	Δ^{199}Hg	Δ^{200}Hg	Δ^{201}Hg
Industrial Era Samples (<200 Years b.p.)															
AG94.1	5.91	12.83	30	50	1960	1980	0.83–0.94	0.87 (3)	−0.11	−0.49	−0.76	−1.13	0.17	0.07	0.08
AG94.1	12.83	18.00	50	73	1937	1960	0.99–1.08	1.05 (3)	−0.15	−0.53	−0.92	−1.27	0.17	0.11	0.04
AG94.1	18.00	21.83	68	85	1925	1942	1.11–1.17	1.14 (2)	−0.19	−0.62	−1.09	−1.48	0.18	0.12	0.02
AG94.1	21.83	28.33	85	114	1896	1925	0.44–1.59	0.77 (4)	−0.12	−0.66	−1.01	−1.65	0.29	0.17	0.22
AG94.1	28.33	30.83	106	122	1888	1904	0.57–2.44	1.31 (2)	−0.24	−0.60	−1.68	−1.87	0.23	0.34	−0.27
AG94.1	30.83	38.33	122	159	1851	1888	0.42–0.61	0.52 (5)	0.13	0.02	−0.17	−0.49	0.25	0.27	0.20
AG94.1	38.33	43.26	155	183	1827	1855	0.56–0.70	0.63 (3)	−0.31	−0.70	−1.28	−1.72	0.13	0.17	0.01
AG94.1	43.26	47.38	179	202	1808	1831	0.86–0.96	0.90 (3)	−0.28	−0.84	−1.47	−2.02	0.23	0.18	0.05
PW05.1	0.75	2.85	6	10	2000	2004	0.54–2.17	1.30 (3)	−0.01	0.16	−0.34	−0.57	0.14	0.45	0.09
PW05.1	2.85	4.84	10	12	1998	2000	0.99–2.57	1.55 (3)	−0.25	0.69	−0.23	0.14	−0.28	0.62	−0.33
PW05.1	4.84	6.19	12	14	1996	1998	1.18–1.54	1.41 (3)	−1.22	0.27	−1.54	−0.51	−1.09	0.52	−1.16
PW05.1	6.19	7.73	14	17	1993	1996	0.39–1.99	0.98 (3)	−0.33	0.38	−0.41	−0.17	−0.29	0.46	−0.28
PW05.1	14.41	17.41	30	36	1974	1980	---	2.81 (1)	−0.39	−0.61	−1.07	−1.39	−0.05	0.08	−0.03
PW05.1	17.41	29.54	36	66	1944	1974	0.17–2.08	0.84	−0.20	−0.21	−0.55	−0.79	0.00	0.18	0.04
PW05.1	29.54	34.42	66	80	1930	1944	0.66–0.93	0.82 (4)	0.06	0.04	−0.07	−0.18	0.10	0.13	0.07
PW05.1	25.64	31.40	64	71	1939	1946	0.79–3.88	2.33 (2)	−0.10	−0.20	−0.43	−0.53	0.04	0.07	−0.04
PW05.1	31.40	38.43	71	92	1918	1939	0.93–1.10	1.02 (3)	−0.22	−0.52	−0.88	−1.44	0.15	0.20	0.21
PN96.2	2.32	18.57	18	92	1918	1992	0.43–0.50	0.45 (3)	−0.36	−0.12	−0.54	−0.38	−0.26	0.08	−0.25
Preindustrial Samples (>200 Years B.P.)															
AG93.2	63.15	81.85	926	2539	–	–	<0.02–0.60	*0.12* (17)	−0.86	−1.17	−1.63	−2.48	−0.24	0.08	0.23
AG93.2	90.95	96.96	3974	4948	–	–	<0.02–0.05	*0.02* (6)	−0.51	−0.38	−1.23	−1.32	−0.18	0.29	−0.24
AG93.2	101.65	108.01	6003	8050	–	–	<0.02–0.10	*0.09* (7)	−0.61	−0.10	0.03	−1.07	−0.34	0.44	0.83
DV99.1	104.16	144.25	1012	3060	–	–	<0.02–0.26	*0.06* (24)	0.39	−0.78	0.44	−1.52	0.77	−0.01	1.58
DV99.1	149.89	155.73	3995	5742	–	–	<0.02–0.22	*0.16* (8)	2.21	−0.44	2.20	−0.91	2.44	0.02	2.88
DV99.1	159.67	163.03	8031	11970	–	–	<0.02–0.42	*0.17* (5)	0.63	−0.52	0.29	−1.09	0.91	0.03	1.12
PN95.4	289.83	312.34	3315	5775	–	–	0.13–0.39	0.20 (7)	−0.48	−0.46	−0.97	−1.24	−0.17	0.16	−0.04
PN95.4	315.02	326.07	6418	11124	–	–	0.11–2.12	0.66 (5)	0.15	0.94	1.46	1.99	−0.35	−0.06	−0.04
PN96.2	106.96	125.77	971	1424	–	–	0.37–0.54	0.48 (5)	−0.17	−0.31	−0.64	−0.84	0.04	0.11	−0.01
PN96.2	125.77	149.67	1424	2806	–	–	0.08–0.66	0.31 (6)	−0.20	−0.42	−0.73	−1.00	0.05	0.09	0.03
PN96.2	155.97	169.43	3888	10617	–	–	0.51–0.59	0.56 (4)	−0.40	−0.59	−1.94	−2.30	0.18	0.57	−0.21

[a]Cores are described in Table 1.
[b]Sample age estimates are approximate only. Years before present (B.P.) refer to the year 2010 A.D.
[c]The [THg] range and weighted mean (where reported) are for *n* samples spanning the same depth intervals in which the Hg isotope ratios were determined. Italicized values are estimates. The mean standard uncertainty (u_c) on [THg] measurements is ± 0.20 ng L^{-1}. For Hg isotopes, estimated uncertainties (±2σ) are as follows: δ^{199}Hg and δ^{200}Hg: ± 0.20‰; δ^{201}Hg and δ^{202}Hg: ± 0.24‰; Δ^{199}Hg: ± 0.18‰; Δ^{200}Hg: ± 0.16‰; and Δ^{201}Hg: ± 0.18‰.

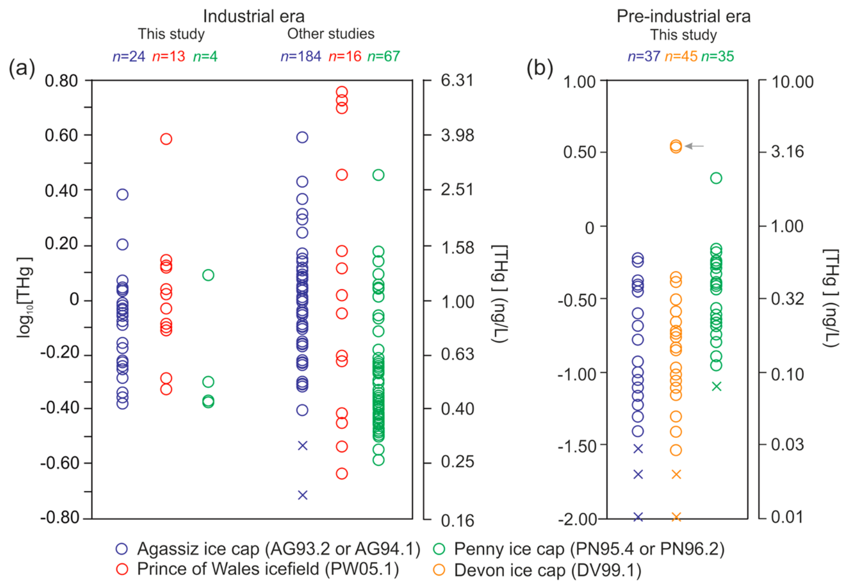

Figure 5. [THg] measured in seasonal snow, firn, and ice core segments from Canadian Arctic ice caps, grouped by age: (a) industrial era samples; (b) preindustrial samples. Data points are color coded as in Figure 2 to identify the ice caps where samples were obtained: Blue = Agassiz ice cap; red = Prince of Wales icefield; orange = Devon ice cap; green = Penny ice cap. Samples with [THg] below the MDL are shown by cross symbols. (a) Results from the present study (inner-core samples only) are compared with data from other published works: Agassiz ice cap [*Zheng*, 2015]; Prince of Wales icefield [*St. Louis et al.*, 2005]; Penny ice cap [*Zdanowicz et al.*, 2013]. Note that several data points in these studies plot below the axis limits ($<$0.15 ng L^{-1}). (b) The data points marked with an arrow are samples from the DV99.1 core which contained visible dust particles (see section 4.4).

cores was not subject to external influences. The similarity of the down-core Δ^{200}Hg and Δ^{201}Hg patterns in the inner and outer cores also suggest that photolytic reactions leading to MIF of Hg in the firn cores during storage were very limited. However, in the remainder of this paper, we limit our presentation and discussion of results to the innermost samples, which we regard as most likely to be pristine, i.e., unchanged since the time of coring.

4.2. Total Mercury

Table 3 gives a summary of results for [THg] and Hg isotope ratios performed as part of this study. The [THg] in the firn and ice core samples (excluding superficial layers) ranged from $<$ 0.05 to ~3.88 ng L^{-1} (Figure 5). In the firn samples from Penny ice cap (core PN96.2), Agassiz ice cap (AG94.1), and the Prince of Wales icefield (PW05.1), [THg] varied between 0.39 and 3.88 ng L^{-1}, which compares well with previous measurements in firn samples collected directly or with a minimum of laboratory manipulations on Penny ice cap (0.51 to 3.48 ng L^{-1} [*Zdanowicz et al.*, 2013]) and Agassiz ice cap (0.50 to 4.00 ng L^{-1} [*Zheng*, 2014]). The weighted mean [THg] in preindustrial ice core samples ranged from 0.05–0.10 ng L^{-1} in the AG93.2 and DV99.1 cores, to 0.45–0.48 ng L^{-1} in the PN95.4 and PN96.2 cores, the latter figures being also consistent with earlier results [*Zdanowicz et al.*, 2013]. The higher [THg] in preindustrial cores from Penny ice cap, compared to those from the High Arctic ice caps, may indicate a larger atmospheric Hg flux into snow at lower Arctic latitudes, either from marine or continental sources, as was suggested before [*Gamberg et al.*, 2015].

For the two Ellesmere Island firn cores that provided most of our industrial era samples, the weighted mean [THg] varied between ~0.84 ng L^{-1} in the AG94.1 core (period ~1808–1980; $n = 25$) and ~ 1.27 ng L^{-1} in the PW05.1 core (period ~1918–2001; $n = 13$). Based on these results, the estimated enhancement factor for [THg] in High Arctic firn since the preindustrial period may range from ~5 to ~10, depending on the assumed mean [THg] in preindustrial layers. For Penny ice cap, near the Arctic Circle (67.3°N) *Zdanowicz et al.* [2015] previously estimated a minimum [THg] enhancement factor of 4. However, translating these estimates in terms of net atmospheric THg deposition rates will require an improved knowledge of preindustrial snow accumulation rates on Canadian Arctic ice caps, which are poorly constrained due to the limited resolution of ice cores, and also of the temporal variability of postdepositional losses of Hg from snow and firn.

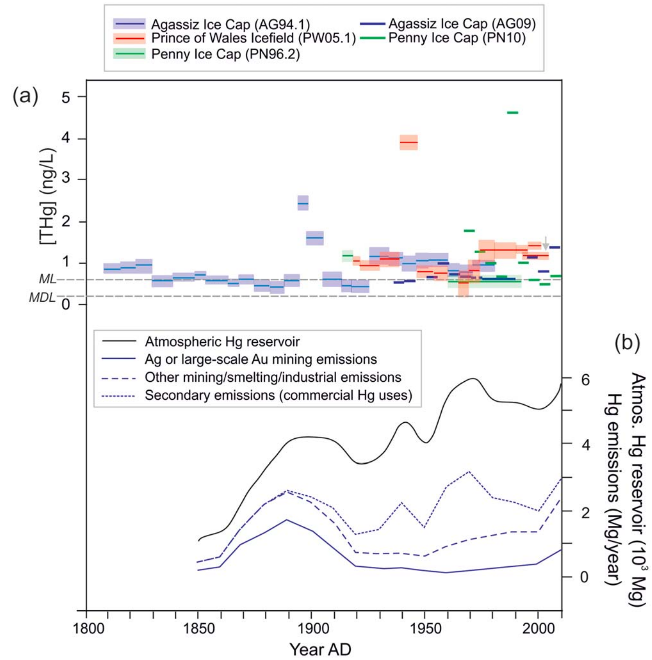

Figure 6. (a) Compilation of [THg] measured in firn and ice core segments from Canadian Arctic ice caps, including data from the AG94.1, PW05.1, and PN96.2 cores (this study), as well as data from two other firn cores drilled on Agassiz ice cap in 2009 (AG09 [*Zheng*, 2014]) and on Penny ice cap in 2010 (PN10 [*Zdanowicz et al*., 2015]). The AG09 and PN10 [THg] data were averaged over ~5 year time steps to facilitate visual comparison with data from other cores. The width of each line segment corresponds to the estimated time span of individual samples or groups of samples, while the height of the shading (for the AG94.1, PW05.1, and PN96.2 cores) denotes the analytical uncertainty of measurements (±2σ). The value marked with an arrow at right is a weighted average of 12 samples taken from a shallow snow/firn core. The estimated method detection limit (MDL = 0.1 ng L^{-1}) and limit of reliable quantitation (ML = 0.5 ng L^{-1}) for [THg] in the AG94.1, PW05.1, and PN96.1 samples are shown as horizontal dashed lines. (b) Reconstructed historical changes in global Hg emissions to the atmosphere since 1800 from various sources and simulated changes in the size of the atmospheric Hg reservoir based on these emissions [*Streets et al*., 2011; *Amos et al*., 2013; *Horowitz et al*., 2014].

Of the three sample sets that span parts of the industrial era, the longest and most continuous is from the AG94.1 core, which is estimated to cover the period 1808 to 1992 (Figure 6). Most [THg] in the nineteenth and early twentieth century parts of this core are ≤1 ng L^{-1} and close to or below the ML (0.2 ng L^{-1}). After ~1920, they rise to a mean of ~1 ng L^{-1}. The [THg] in the AG94.1 core are closely comparable with measurements made by *Zheng* [2014] in a 15 m firn core from another site on Agassiz ice cap (AG09) and spanning the period 1936–2009. There is a ~40 year overlap between the two data sets, over which [THg] in the AG94.1 core are only slightly higher (by a mean of ~0.3 ng L^{-1}) than in the AG09 core. However, the difference is not statistically meaningful and could easily be ascribed to local differences in snow accumulation conditions at the two sites [*Fisher et al*., 1995]. The PW05.1 core from central Ellesmere Island is estimated to span an ~82 year period starting in ~1918. Most [THg] in this core also fall within the range measured in the AG94.1 and AG09 cores. The PN96.2 core provided four samples only, dated between ~1914 and 1992. The [THg] in these samples ranged from 0.43 to 1.22 ng L^{-1}. These samples overlap slightly with a firn core (PN10) drilled from the same site and spanning the interval ~1970–2010, in which [THg] were found to be mostly ≤5 ng L^{-1}, averaging ~1 ng L^{-1} [*Zdanowicz et al*., 2015].

There has been some disagreement in recent literature about the possible magnitude of historical nineteenth century mining Hg emissions to the atmosphere and their global impact [*Engström et al*., 2014; *Beal et al*., 2015; *Zhang et al*., 2014]. Only two samples of our AG94.1 firn core, dating from the interval ~1893–1904, were found to have [THg] in excess of 1.5 ng L^{-1}, markedly higher than the mean for the whole core (~0.84 ng L^{-1}) (Figure 6). Thus, unlike in glaciers of the midcontinental U.S. [*Schuster et al*., 2002], we found no evidence for a decade-long period of sustained higher Hg deposition on Agassiz ice cap that could be unequivocally ascribed to enhanced mining Hg emissions during the nineteenth century Au/Ag mining boom. This seems to support the view, advanced or endorsed by some

Table 4. [MeHg] Measured in Selected Firn and Ice Core Samples From the Canadian Arctic[a]

Core	Time Interval (Estimated Years b.p.) From	To	Weighted Mean [THg] (ng L^{-1})	[MeHg] (ng L^{-1})	$\frac{[MeHg]}{[THg]}$ (%)
AG94.1	136	35	1.94	0.02	1
AG93.2	2540	1972	0.12	*0.02*	*12*
	4740	4090	0.27	*0.01*	*5*
	7661	6492	0.26	*0.02*	*6*
DV99.1	1205	1019	0.09	*0.01*	*10*
	2357	2256	0.32	*0.01*	*3*
	5742	2674	0.29	*0.01*	*5*
PN95.4	4437	4183	0.22	*0.01*	*4*
	6214	5775	0.16	*0.01*	*7*
	7922	7370	0.33	0.07	17

[a]The fraction of THg as MeHg was estimated from the weighted mean [THg] in the samples that were combined for MeHg analysis. Figures in italics denote [MeHg] that were below the MDL (0.02 ng L^{-1}). The corresponding [MeHg]/[THg] (also italicized) are estimates.

[*Engström et al.*, 2014; *Beal et al.*, 2015; *Zhang et al.*, 2014], that the impact of these emissions on atmospheric Hg deposition rates at high latitudes was limited.

4.3. Methylmercury

Table 4 gives results of the [MeHg] analyses performed on firn and ice core samples. Most values were extremely low ($\leq$0.02 ng L^{-1}), and only one sample contained [MeHg] near the ML of 0.06 ng L^{-1}. An attempt was made to estimate the percentage of MeHg in THg using the weighted average [THg] in the subsamples that had been combined for MeHg analyses. Results indicate that MeHg typically accounts for $\ll$20% of THg accumulation in glacial firn and ice, which is consistent with previous findings from other snow/firn/ice measurements [*Gamberg et al.*, 2015]. This does not rule out a possible contribution of methylated Hg from marine sources to Hg deposition on Canadian Arctic ice caps [e.g., *St. Louis et al.*, 2005, 2007], but it suggests that this is either very small or quickly lost from the snowpack by photolytic demethylation and subsequent evasion as $Hg^0_{(g)}$. It is noteworthy, but maybe coincidental, that the core sample with the highest [MeHg] came from the southernmost ice cap of all (Penny) and is estimated to date to the early Holocene (ca. 8000–7000 years B.P.), a time when the southern Baffin Island region probably experienced much warmer conditions and reduced sea ice coverage than today [*Briner et al.*, 2016].

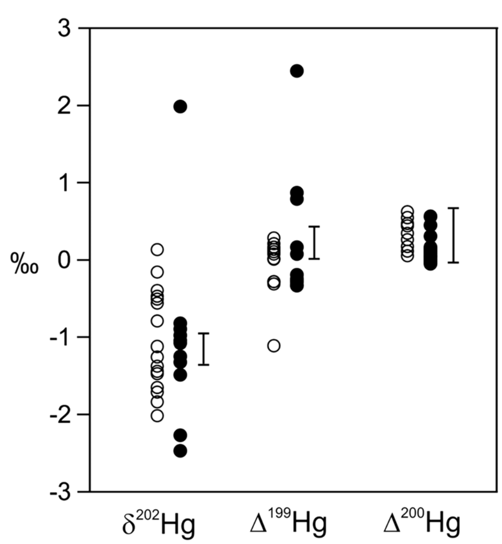

Figure 7. Range of Hg isotope composition in industrial age (open circles) and preindustrial (full circles) firn or ice core samples from Canadian Arctic ice caps (n = 29). Mean analytical uncertainties (±2σ) for δ^{202}Hg, Δ^{199}Hg, and Δ^{200}Hg are indicated with an error bar.

4.4. Hg Isotope Composition of Preindustrial Versus Industrial Era Samples

Figure 7 shows the range of Hg isotopic compositions (δ^{202}Hg, Δ^{199}Hg, and Δ^{200}Hg) in all Canadian Arctic firn and ice core samples (n = 29). The widest range of variations is observed for δ^{202}Hg (−2.48 to 1.99‰) in both industrial age and preindustrial samples and for Δ^{199}Hg (−1.09 to 2.44‰) in preindustrial samples. The range of Δ^{200}Hg variations is comparatively limited (−0.06 to 0.62‰) and nearly identical in both sample groups. With the exception of a single sample from core PN95.4, preindustrial ice core samples have δ^{202}Hg close to or below −1‰ (weighted mean = −1.53 ± 0.09‰), while industrial era samples have a relatively even spread of δ^{202}Hg values ranging from −2.02 to 0.14‰ (weighted

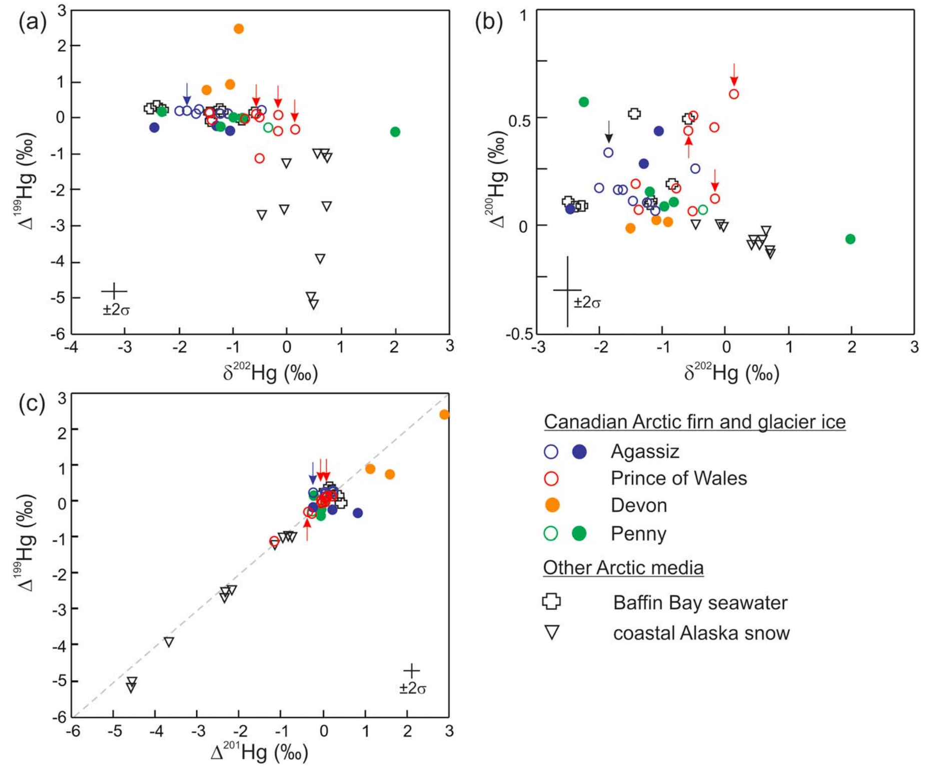

Figure 8. Hg isotopic signatures (δ^{202}Hg, Δ^{199}Hg, Δ^{200}Hg, and Δ^{201}Hg) measured in Canadian Arctic glacial firn and ice cores. Open circles = industrial age samples; full circles = preindustrial age samples. Results are compared with published data from surface seawater of northern Baffin Bay [*Štrok et al.*, 2015] and Alaskan snowfall and coastal snow [*Sherman et al.*, 2010, 2012a]. Points identified with an arrow correspond to those samples for which the zeta score for [THg] was >2 (see section 3.4).

mean = −0.94 ± 0.06‰) (Figure 7). With respect to Δ^{199}Hg, the weighted means for samples of preindustrial age (−0.08 ± 0.07‰) are identical, within error, to that of industrial era samples (−0.07 ± 0.04‰). However, there is a wider spread of Δ^{199}Hg values in the preindustrial ice core segments, which is largely accounted for by three samples in the DV99.1 core with Δ^{199}Hg equal to 0.77, 0.91, and 2.44‰ (Δ^{201}Hg: 1.58, 1.12, and 2.88‰). These samples are discussed later.

The speciation of Hg found in polar snowpacks is still poorly known, and hardly any data exist from glacier firn and ice cores, except for some estimates of methylated Hg [*Zdanowicz et al.*, 2013; *Gamberg et al.*, 2015]. It is currently thought that owing to the low precipitation rates in the Arctic, atmospheric Hg is primarily deposited in terrestrial snow as gaseous elemental Hg ($Hg^0_{(g)}$), as reactive gaseous Hg ($H^{II}_{(g)}$), or as particulate-bound Hg ($Hg_{(p)}$, or PHg) [*Steffen et al.*, 2008, 2015]. One study conducted in the Canadian High Arctic suggests that PHg could account for as much as ~60% of total deposition [*Poulain et al.*, 2007]. Knowledge of Hg contributions from wet deposition, and of Hg speciation associated with this form of deposition, is hampered by the lack of adequate measurements in the Arctic region. The values of δ^{202}Hg, Δ^{199}Hg, and Δ^{200}Hg determined in our firn and ice core samples overlap with those of $Hg^0_{(g)}$ measured in a few samples collected by *Sherman et al.* [2010] in Alaska, but they also fall close to or within the range observed in present-day surface seawater of northern Baffin Bay (Figure 8) [*Štrok et al.*, 2015]. This area is known to be a major source for precipitating moisture and marine aerosols deposited on Canadian High Arctic ice caps [*Koerner*, 1979; *Kinnard et al.*, 2006]. The similarity of isotopic signatures suggests that some fraction of the Hg which accumulates in firn on these ice caps could be issued directly (i.e., with little or no fractionation) from this nearby marine source, possibly as $Hg^{II}_{(aq)}$ in aerosol form, or in precipitation. High enrichments of Hg relative to soil have been found in lichen growing at coastal sites of Bathurst and Devon Islands lying close to polynyas, pointing to a potentially important marine source of local atmospheric Hg deposition in this region [*St. Pierre et al.*, 2015]. Some of this marine Hg may be emitted as MeHg [e.g., *St. Louis et al.*, 2005, 2007], but as our [MeHg] data suggest, this appears to be a very small fraction of the THg accumulated on glaciers.

The predominantly positive Δ^{200}Hg measured in our firn and ice core samples include several values that are more than 2σ above 0 (0.34 to 0.62‰). These findings add to a growing pool of observations, mostly from precipitation but also from seawater, which attest to the occurrence of MIF of even-numbered Hg isotopes in the environment [e.g., *Gratz et al*., 2010; *Chen et al*., 2012; *Štrok et al*., 2015]. While the responsible mechanism(s) remain uncertain, it has been speculated that Hg carrying positive Δ^{200}Hg anomalies originates through oxidation of Hg^0 in the upper atmosphere and is then supplied to the troposphere by stratospheric air intrusions, which are more common at high latitudes [*Cai and Chen*, 2016]. The data presented here offer some support for this hypothesis, although the maximum Δ^{200}Hg measured in our samples (0.62‰) does not exceed that measured in midlatitude precipitation [*Chen et al*., 2012].

Presently, the only other published data on Hg isotopes in Arctic precipitation come from snowfall and surface snow samples collected in coastal Alaska (some on sea ice) by *Sherman et al*. [2010, 2012a]. *Chen et al*. [2012] also reported data from a single surface snow sample collected in northern Greenland, but at present this remains an isolated value. The isotopic composition of Hg in Canadian Arctic firn and ice core samples is distinct from the Alaskan snow samples of *Sherman et al*. [2012a] (Figure 8). Most δ^{202}Hg values in the firn/ice samples are clearly negative (down to −2.48‰), while the Δ^{199}Hg and Δ^{200}Hg values are either close to 0 or clearly positive (up to 2.44‰). The pattern observed in the Alaskan snow samples is almost completely opposite. These samples were collected in March 2006 and 2009, during periods of springtime atmospheric Hg depletion events (AMDE) [*Schroeder et al*., 1998]. The Hg deposited in Arctic snow during these events undergoes rapid postdepositional photochemical reduction and evasion from the snowpack [*Steffen et al*., 2008; *Durnford and Dastoor*, 2011]. These processes can modify the concentration and speciation of Hg in the uppermost layers (typically, a few centimeters) of the snowpack [*Durnford and Dastoor*, 2011; *Mann et al*., 2014]. *Sherman et al*. [2010] have shown that photoreduction of Hg^{II} and subsequent evasion of $Hg^0_{(g)}$ from Arctic snow is accompanied by both MDF and MIF. With respect to MDF, the lighter Hg isotopes are preferentially lost by evasion, such that the remaining Hg in snow becomes isotopically heavier, i.e., evolves toward more positive δ^{202}Hg values. During MIF, it is the odd-numbered isotopes that are being preferentially reduced and emitted, and this imprints the remaining Hg in snow with increasingly negative Δ^{199}Hg values (down to −5.08‰ in drifted snow) [*Sherman et al*., 2010].

Atmospheric bromine oxidants (Br and BrO), which are key participants in AMDE, occur over the Canadian Arctic islands during springtime, as shown by satellite measurements [*Simpson et al*., 2007]. It is therefore likely that at least some of the Hg found in Canadian Arctic ice caps is deposited during AMDEs, but our Hg isotope measurements indicate that this is probably a minor contribution to net THg accumulation in firn and ice. Unlike *Sherman et al*.'s [2010, 2012a] snow samples from coastal Alaska, our snow and ice core samples represent aged precipitation that accumulated over decades to millennia. The Hg isotopic signature of each sample is therefore a weighted average of the composition of numerous subannual layers, of which those formed in early springtime, the main period of AMDE occurrence, only represent a relatively small fraction, as most snow accumulation on Canadian Arctic occurs in late summer, autumn, and late spring [*Zdanowicz et al*., 2013]. A consequence of this seasonality is that it probably does not favor the preservation of AMDE-deposited Hg in snow on Arctic ice caps, which can be photoreduced and reemitted to the atmosphere before it can be buried below the photolytic zone.

While the range of Hg isotope compositions in Canadian High Arctic firn and glacier ice resembles that in Baffin Bay seawater, it also overlaps with that in contemporary precipitation collected in midlatitude regions of North America and China, regions which are affected by Hg emissions from point sources such as coal-fired utility boilers or nonferrous metal smelters (Figure 9; data from *Gratz et al*. [2010], *Chen et al*. [2012], *Sherman et al*. [2012b, 2015], *Demers et al*. [2013, 2015], and *Wang et al*. [2015]). The similarity in these isotopic signatures raises the possibility of contributions from distant anthropogenic emission point sources to Hg accumulation on Canadian Arctic ice caps in historical times. Simulations using global transport models of atmospheric Hg indicate that long-range transport of $Hg^0_{(g)}$ from midlatitude/low-latitude pollution source(s) to the Canadian Arctic can occur from all Northern Hemisphere regions, Asia being currently predominant, partly on account of the intense utilization of coal as an energy source in China [*Durnford et al*., 2010].

Primary sources of Hg emissions for which detailed stable isotope data are presently available include coals [*Sun et al*., 2014, and references therein], Hg hydrothermal ores [*Smith et al*., 2014; *Stetson et al*., 2009; *Wiederhold et al*., 2013; *Yin et al*., 2013], and volatiles emitted from volcanic vents [*Zambardi et al*., 2009;

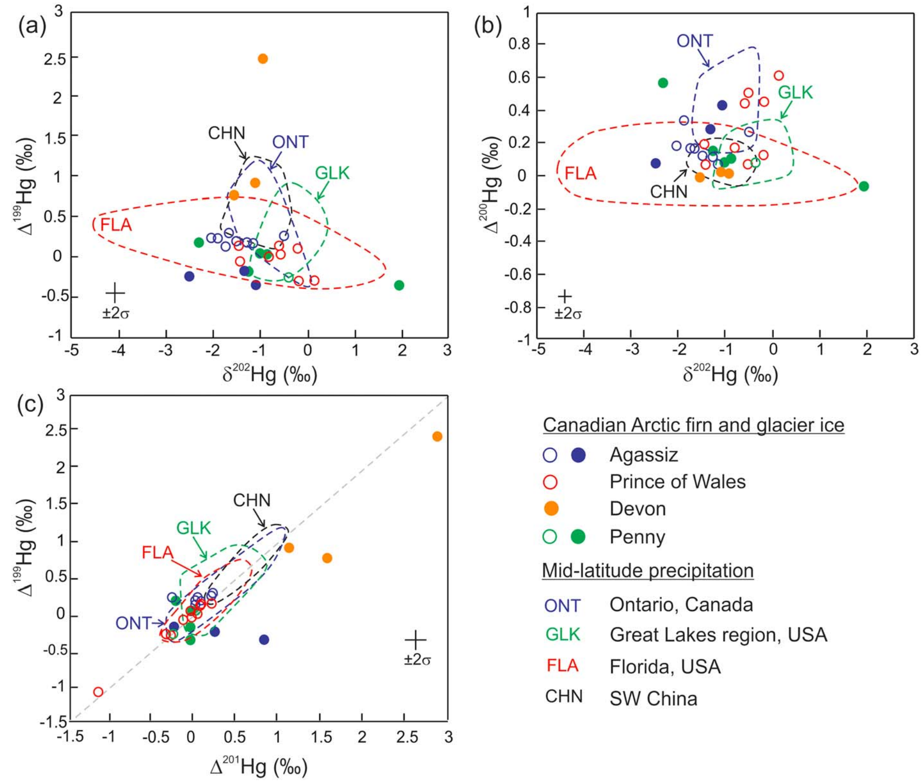

Figure 9. Hg isotopic signatures (δ^{202}Hg, Δ^{199}Hg, Δ^{200}Hg, and Δ^{201}Hg) measured in Canadian Arctic glacial firn and ice cores (circles; as in Figure 8) compared with the range of signatures in midlatitude precipitation impacted by anthropogenic Hg emission sources: Ontario, Canada [*Chen et al.*, 2012]; Great Lakes region, USA [*Demers et al.*,2013; *Gratz et al.*, 2010; *Sherman et al.*, 2015]; Florida, USA [*Sherman et al.*, 2012c; *Demers et al.*, 2015]; and southwestern China [*Wang et al.*, 2015]. Note that a few outliers were omitted from these data.

Sun et al., 2016]. The isotopic composition of atmospheric Hg emitted from metal smelters or metallurgical plants is poorly documented, but that of smelter-impacted soils and sediments can be used as a proxy [*Sonke et al.*, 2010; *Estrade et al.*, 2011; *Gray et al.*, 2013; *Ma et al.*, 2013]. The range of Hg isotope compositions in these sources overlap with each other and also with that of many (albeit not all) of our Canadian firn and ice core samples, of both preindustrial and industrial era age (Figure 10). Such findings must of course be interpreted with caution, since the MDF signature of atmospheric Hg emitted from low-latitude or midlatitude sources may be modified by fractionation processes prior to or during long-range transport to polar latitudes. That being said, for several large anthropogenic sources, such as ferrous/nonferrous metal smelting, or the production of liquid Hg^0, current data suggest that emissions to the atmosphere bear a strong isotopic resemblance to the source materials [*Sun et al.*, 2016, and references therein].

The extent to which the Hg isotopic composition of our Arctic firn and ice cores overlaps with that of potential Hg emission sources can be examined more closely through a principal component analysis (PCA) applied to the isotopic data displayed in Figures 8 and 9. The PCA identifies two dominant factors of variability in the data, the first one (PC1) corresponding almost entirely to δ^{202}Hg and the second one (PC2) being primarily linked to covariations of Δ^{199}Hg and Δ^{201}Hg. Together, these two factors account for 99% of the overall variance in the data (Table 5). The variability accounted for by Δ^{200}Hg is comparatively very small.

Most Arctic firn and ice core samples plot in a relatively restricted field within the bivariate space defined by PC1 and PC2, in which they overlap with many, but not all, of the other media or Hg sources (Figure 11). The degree of overlap is largest with some of the Hg ore and coal data and with the Baffin Bay seawater data. The poorest match is with the Alaska snow samples of *Sherman et al.* [2010, 2012a], with the smelter-impacted sediment, and with some of the midlatitude precipitation data with large positive Δ^{199}Hg and Δ^{201}Hg signatures. These results do not allow specific source types or source region contributions of Hg in Arctic firn and ice to be unambiguously identified or discriminated. However, they offer some insights into the more, or less, likely candidates.

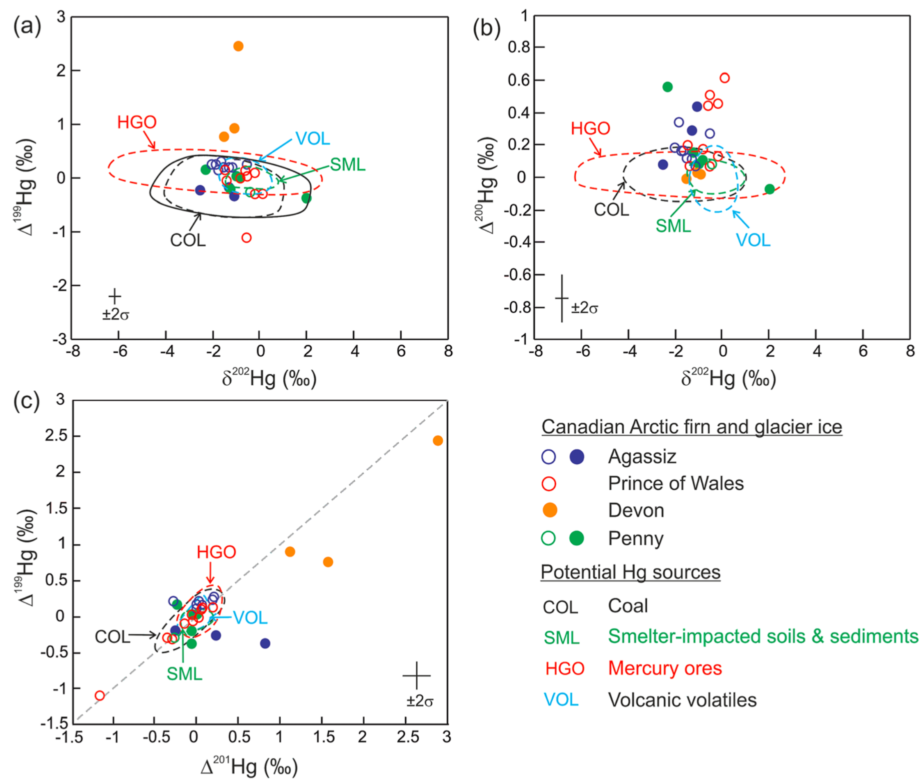

Figure 10. Hg isotopic signatures (δ^{202}Hg, Δ^{199}Hg, Δ^{200}Hg, and Δ^{201}Hg) measured in Canadian Arctic glacial firn and ice cores (circles; as in Figure 8) compared with the range of signatures in primary sources of Hg emissions: Coal and related deposits [*Sun et al.*, 2014, and references therein], smelter-impacted soils and sediments [*Sonke et al.*, 2010; *Estrade et al.*, 2011; *Gray et al.*, 2013; *Ma et al.*, 2013], Hg hydrothermal ores [*Smith et al.*, 2014; *Stetson et al.*, 2009; *Wiederhold et al.*, 2013; *Yin et al.*, 2013], and volatiles from volcanic emissions [*Zambardi et al.*, 2009; *Sun et al.*, 2016]. (a) For coal, the dashed contour encompasses Hg isotope signatures in coal deposits, while the full circle encompasses the possible range of signatures in coal-derived atmospheric Hg, assuming possible MDF between −0.5 and 1‰ for δ^{202}Hg [*Sun et al.*, 2016]. Note that a few outliers were omitted from these data.

The Δ^{199}Hg/Δ^{201}Hg ratio in environmental sample media can be used as an indicator of the type of MIF process affecting their Hg isotopic composition [*Blum et al.*, 2014]. A robust least squares linear regression of Δ^{199}Hg over Δ^{201}Hg fitted to all our firn and ice samples yields a slope of 0.85 ($R^2 = 0.93$; 95% confidence limits: ± 0.08). If the samples from core DV99.1 with the largest positive Δ^{199}Hg and Δ^{201}Hg are excluded, the regression slope is 0.99 ($R^2 = 0.81$; 95% confidence limits: ± 0.17), which is identical, within error, to the expected mean Δ^{199}Hg/Δ^{201}Hg ratio of 1.0 for Hg^{II} following photoreduction [*Bergquist and Blum*, 2007]. This MIF signature in accumulated firn and ice could be derived from that of precipitation and/or could be inherited from postdepositional photoreduction of Hg^{II} in the snowpack prior to burial.

The three DV99.1 ice core samples with large positive Δ^{199}Hg and Δ^{201}Hg are highly unusual since such high MIF signatures have so far been reported primarily in aquatic (freshwater or marine) biological samples such

Table 5. Results of Principal Component Analysis[a]

Component	PC1	PC2	PC3	PC4
Variance (%)	*74*	*25*	*1*	*0*
Cumulative variance (%)	*74*	*99*	*100*	*100*
		Factor loadings		
δ^{202}Hg	0.98	0.22	0.01	−0.02
Δ^{199}Hg	−0.17	0.70	−0.04	−0.69
Δ^{200}Hg	−0.02	0.05	1.00	−0.01
Δ^{201}Hg	−0.14	0.68	−0.03	0.72

[a]PCA analysis shown in Figure 11 was applied to data displayed in Figures 8–10.

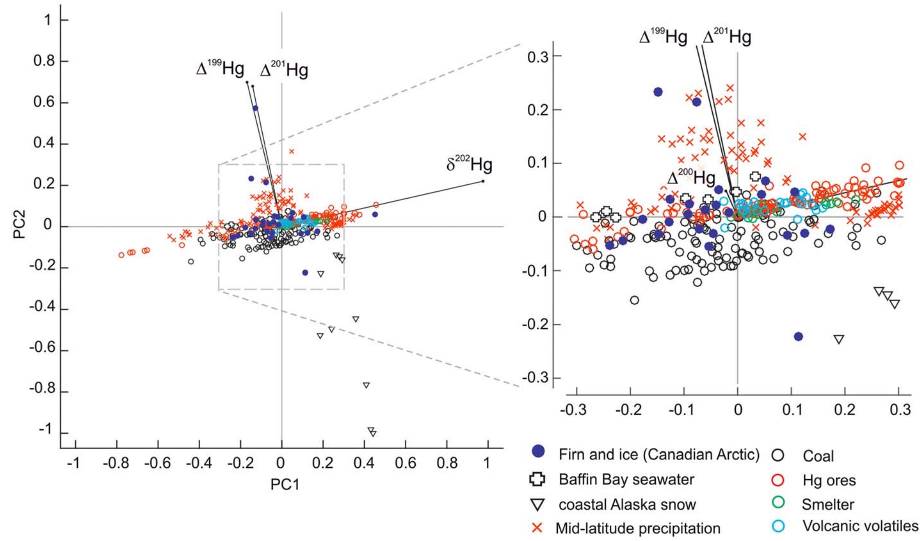

Figure 11. Biplot of two first principal components (PC1 and PC2) of variability in the Hg stable isotope data from Figures 8 to 10. Values on the two axes correspond to PC loadings for individual observations.

as fish or seabird eggs and only rarely in precipitation [*Blum et al*., 2014, and references therein]. If these unusual signatures in the DV99.1 core are genuine, how could they be accounted for? Recently, *Rose et al*. [2015] experimentally obtained Δ^{199}Hg as high as 2.42‰ (Δ^{201}Hg up to 2.35‰) by photoreduction of an aqueous Hg^{II} solution enriched with dissolved organic matter, which suggests at least one abiotic process by which such isotopic signatures might be produced in the environment.

Unlike the other cores listed in Table 1, the DV99.1 core was recovered from a site which is not at the summit of the ice cap (~1930 m asl) but lies some 25 km to the east of it, at an altitude of ~1750 m asl, and relatively close to the present-day lower limit of the accumulation zone, i.e., near the ice cap's equilibrium line in this area. Conceivably, under the warmer climate conditions that prevailed during much of the Early and Mid-Holocene across the Canadian High Arctic (Figure 2), the equilibrium line on the northeastern sector of Devon ice cap may have retreated above its present position, bringing the DV99.1 coring site closer to, or into, the ablation zone. There, cryoconite holes and/or meltwater ponds may have formed during summer, in which soil-derived, windblown silt accumulated, and cyanobacteria and algae grew, as observed nowadays on the marginal zone of polar ice sheets [e.g., *Barker et al*., 2006; *Stibal et al*., 2010]. Such environments, where organic carbon can readily accumulate, may have offered, during earlier, warmer parts of the Holocene, suitable conditions at the surface of Devon ice cap for the type of aqueous Hg^{II} photoreduction process observed by *Rose et al*. [2015]. A subsequent lowering of the equilibrium line altitude during renewed expansion of Devon ice cap in the Late Holocene could have ensured the preservation of firn or superimposed ice strata bearing the unusual Δ^{199}Hg and Δ^{201}Hg signatures identified in the DV99.1 core.

Possible supporting evidence for the scenario described above was provided by the finding of single and clustered soil particles, some up to several hundred micrometers in diameter, imbedded in DV99.1 ice core samples from depths between ~162 and 163 m, i.e., in the depth range where some of the anomalously high Δ^{199}Hg and Δ^{201}Hg values were measured (Table 3). The core sample in which these particles were identified had also unusually high [THg] of 3.43 ± 0.03 (2σ; $n = 3$ replicate analyses). Particles filtered from the meltwater were examined at the University of Ottawa and Canadian Museum of Nature MicroAnalysis Laboratory using an analytical scanning electron microscope equipped with an energy-dispersive X-ray microanalyzer (SEM-EDX) and found to be composed of common soil-forming minerals such as quartz, feldspars, clays, Fe oxides, pyroxenes, and amphiboles, as well as some organic matter (Figure S1). The presence of such particles supports the view that the site where the DV99.1 core was drilled was, at some time during the early or mid-Holocene, exposed to the surficial accumulation of windblown dust and organic matter.

4.5. Hg Isotope Variations in Firn During the Industrial Era

The data obtained from firn cores AG94.1, PW05.1, and PN96.2 allow us to examine how the isotopic composition of THg in accumulating snow on Canadian Arctic glaciers evolved since the early nineteenth century. The longest data set is from core AG94.1, whereas samples from cores PW05.1 and PN96.2 in which Hg isotopic ratios were determined only cover parts of the twentieth century (Figure 12). Because the AG94.1 record is the longest and most continuous, we focus the remainder of the discussion on it. Two features in this record are especially noteworthy. The first is a gradual shift in δ^{202}Hg of ~ +1‰ from the nineteenth to late twentieth centuries. The second is a large, but transient, positive δ^{202}Hg offset (from −1.72 to −0.49‰) between the 1850s and 1890s. Some known postdepositional processes, including deep air convection, gravitational settling, and thermal diffusion, can produce stable isotope variations in firn gases [*Craig et al.*, 1988; *Severinghaus et al.*, 2001]. However, such processes would only affect the isotopic composition of interstitial $Hg^0_{(g)}$, which, as stated earlier, likely represents a minor fraction of the measured [THg] in the firn. Thus, they seem inadequate to account for the observed δ^{202}Hg variations in the AG94.1 core.

Recently, *Sun et al*. [2016] modeled the evolving stable isotope composition of global anthropogenic Hg emissions to the atmosphere since the midnineteenth century. Their modeling results show that from 1850 until 2010, the δ^{202}Hg of these emissions evolved toward increasingly positive values as a result of historical changes in predominant Hg sources to the atmosphere. This change would have been largest for gaseous Hg (in both elemental or oxidized forms) or for Hg "by-product" emissions associated with Cu, Zn, and Pb smelting, Fe and steel manufacturing, liquid Hg^0 production, cement manufacturing, the combustion of coal and oil, and large-scale Au mining without Hg amalgamation [*Sun et al*., 2016]. Remarkably, the positive trend in δ^{202}Hg measured in the AG94.1 firn core over the period 1850–2010 is of comparable magnitude (~1.0‰) to that predicted by *Sun et al*.'s [2016] model for all by-product Hg emissions (Figure 12). The Δ^{199}Hg in the AG94.1 core show comparatively minor temporal variations during this period, which also agrees (within error bounds) with *Sun et al*.'s [2016] modeling results.

These findings suggest that the secular trend toward more positive δ^{202}Hg observed in the AG94.1 core may actually reflect the historical evolution in the isotopic composition of the global atmospheric Hg reservoir. Calculations by *Streets et al*. [2011] indicate that the size of this reservoir increased through the nineteenth and twentieth centuries as a result of cumulative anthropogenic mining and industrial emissions (Figure 6). *Sun et al*.'s [2016] modeling results imply that as the atmospheric Hg reservoir grew, its isotopic composition evolved toward a more positive mean δ^{202}Hg owing to the changing nature of atmospheric Hg emissions. We speculate that the pool of atmospheric Hg in the High Arctic evolved in parallel, with an increasingly large anthropogenic fraction and increasingly positive mean δ^{202}Hg signature. This evolution of the atmospheric Hg pool was subsequently recorded in the δ^{202}Hg of accumulated THg in snow on Canadian High Arctic ice caps. This would not necessarily require a large increase in net THg deposition to snow but only that the fraction of anthropogenic THg deposited in snow be sufficiently large to produce the observed change in the δ^{202}Hg of firn on Agassiz ice cap. *Sun et al*. [2016] also modeled the isotopic evolution of *total* Hg emissions, including those from "intentional Hg use" activities such as large-scale Au and/or Ag mining, since the midnineteenth century [*Amos et al*., 2013; *Horowitz et al*., 2014]. The predicted historical δ^{202}Hg trend for total Hg emissions is weaker than that observed for by-product emissions and shows a poorer correspondence with the AG94.1 δ^{202}Hg data (Figure 12). One possible implication is that over a secular time scale, cumulative by-product Hg emissions to the atmosphere had a relatively larger impact on the Hg isotope composition of accumulated High Arctic snow than did emissions from intentional Hg use activities.

It is tempting to establish a link between the large positive δ^{202}Hg offset in the AG94.1 core during the middle/late nineteenth century (Figure 12) and the period of enhanced atmospheric Hg emissions in North America at that time [*Streets et al*., 2011]. Conceivably, a large but transient "pulse" of Hg, emitted during the nineteenth century Au/Ag mining boom, could have imprinted the atmospheric Hg reservoir with an unusually positive δ^{202}Hg signature that persisted for a few decades, until this was mixed and diluted by subsequent Hg emissions with different mean isotopic compositions. The estimated Hg recovery after preconcentration for the core sample with the unusually positive δ^{202}Hg value was 97.1 ± 10%, which seems to rule out external contamination in the preconcentration procedure, although it does not rule out prior contamination, for example, when melting the outer layers of the core. However, the δ^{202}Hg of global anthropogenic THg emissions modeled by *Sun et al*. [2016] for

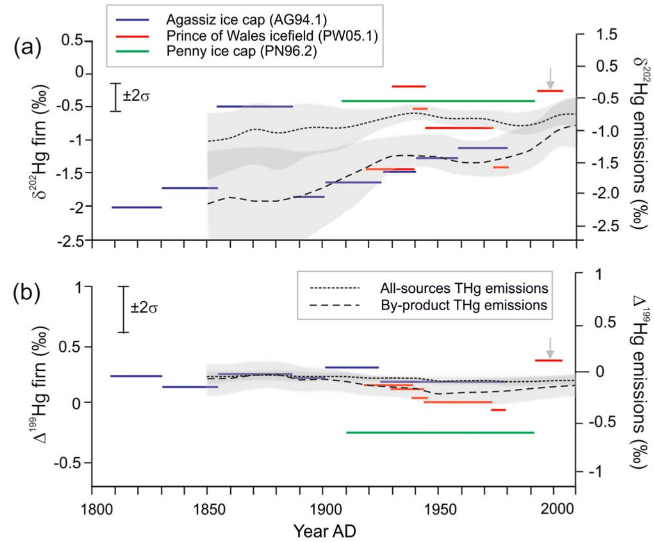

Figure 12. Historical variations in the isotopic composition of (a) δ^{202}Hg and (b) Δ^{199}Hg recorded in snow and firn on Canadian High Arctic ice caps over the past ~200 years, compared with modeled historical variations in the δ^{202}Hg and Δ^{199}Hg of total atmospheric Hg emissions (THg) between 1850 and 2010 [*Sun et al.*, 2016]. For the snow and firn core data, the width of each line segment corresponds to the estimated time span of individual samples or group of samples. Values marked with an arrow at right are weighted averages of four samples taken from a shallow snow core. For the modeled atmospheric data, "by-product" emissions include Cu, Zn and Pb smelting, Fe and steel manufacturing, liquid Hg^0 production, cement manufacturing, combustion of coal and oil, and large-scale gold mining without Hg amalgamation. The shaded areas around each curve denote their 90% confidence bounds.

the middle to late nineteenth century period only shows a modest positive shift of ~0.1‰ at that time (albeit with large uncertainties; Figure 12). Furthermore, the AG94.1 core shows no evidence for sustained higher [THg] between the 1850s and 1890s (Figure 6), which is contrary to expectations if there had been a substantially larger input of global anthropogenic Hg during this period. Hence at present, this single unusual δ^{202}Hg signature in the AG94.1 core remains an unexplained outlier, which could not be replicated due to the limited sample volume available. Nonetheless, its synchronicity with the postulated period of nineteenth century peak Ag/Au mining emissions remains striking and suggestive and deserves further investigation.

5. Conclusions

In this study, we have reported on a first data set of historical variations of the stable isotope composition of Hg in the Arctic environment recorded in glacier firn and ice cores. Our results may help to better constrain the variability of Hg isotopic signatures in the Arctic atmosphere and cryosphere under both present and past environmental conditions and support future modeling efforts of the global Hg biogeochemical cycle. Several key findings emerged from our investigation:

1. Measurements in High Arctic firn and ice cores of various ages show that overall, [THg] increased from close to or less than 0.5 ng L^{-1} during the preindustrial part of the Holocene to mean levels on the order of ~0.8–1.2 ng L^{-1} during the modern industrial era (the past ~200 years). Although the exact magnitude of the [THg] enhancement since the onset of the industrial era is difficult to ascertain, our data suggests that it was on the order of 5–10 times.
2. The Hg isotope composition of accumulated snow on Arctic ice caps strongly differs from that in the springtime snow cover of coastal Alaska. It has been suggested that the distinctive MIF signature of odd-numbered Hg isotopes (Δ^{199}Hg and Δ^{201}Hg) in coastal Arctic snow could be used as a tracer of AMDE-deposited Hg in aquatic ecosystems [*Sherman et al.*, 2010]. Our results, however, indicate that meltwater from glaciers and Arctic ice caps that enters such ecosystems [e.g., *Søndergaard et al.*, 2015] will likely carry Hg with a different isotopic imprint. This fact needs to be accounted for when attempting to track the fate of Hg in Arctic aquatic ecosystems using Hg isotopes.
3. The range of Hg isotopic compositions measured in firn and glacier ice of Canadian Arctic ice caps overlaps with that of several possible known sources, some proximal, such as surface seawater in northern Baffin Bay, and some distant, such as volcanic emissions, or anthropogenic Hg emissions from various industrial processes. However, the degree of overlap makes it impossible, at present, to confidently discriminate between these sources (or source regions) using Hg isotopic data alone.
4. Historical variations of δ^{202}Hg over the past ~200 years recorded in the AG94.1 core from Agassiz ice cap (northern Ellesmere Island) display a gradual positive shift of ~1‰ from the nineteenth to the late twentieth centuries, which parallels the estimated trend in the δ^{202}Hg of industrial by-product THg emissions to the atmosphere over the same period [*Sun et al.*, 2016]. We hypothesize that the δ^{202}Hg of firn

accumulated on Agassiz ice cap reflects the isotopic evolution of the atmospheric Hg pool in the High Arctic in response to growing anthropogenic emissions.

The findings presented here must be considered with some caution, given the nature of the sample material used (archived cores) and limited number of isotopic measurements, and will need to be verified and validated through further studies. An important source of uncertainty concerns postdepositional transformations in the atmospheric Hg record preserved in firn and ice. On all large Canadian Arctic ice caps, as in Greenland, the industrial period is recorded in firn layers, while the preindustrial era is mostly recorded in glacier ice. This raises the question as to whether changes may occur during the transformation of firn to ice that could modify the Hg content of firn and/or its isotopic composition. With respect to interstitial $Hg^0_{(g)}$ in firn, evidence from central Greenland [*Faïn et al*., 2008] indicates that the mixing ratio in firn evolves during burial to eventually approach the mean concentration in air above the snow surface, i.e., the short-term diel or seasonal fluctuations induced by snow-air exchanges are smoothed out during firn burial. As mentioned earlier, there are also some known mechanisms that can modify the mixing ratio or isotopic composition of gases during occlusion [*Craig et al*., 1988; *Severinghaus et al*., 2001]. We consider it likely that $Hg^0_{(g)}$ represents but a minor fraction of the THg in firn and glacier ice, so it seems unlikely that these mechanisms would profoundly modify the MDF signature of THg. Presently, as far as MIF is concerned, photochemical processes are the only known processes that can induce significant fractionation in Hg isotopes. These processes can only operate in the uppermost layers of the snowpack (typically a few tens of centimeters) [*Mann et al*., 2014], where the actinic flux is large enough. They should therefore not induce major differences between firn and ice. Redox reactions involving changes in Hg speciation in snow have also been documented under dark conditions, but it is presently unknown if these might affect the isotopic composition of Hg [*Ferrari et al*., 2004; *O'Concubhair et al*., 2012].

At present, to the best of our knowledge, the only other historical records of Hg isotopic composition available from the Arctic region come from sediment cores extracted from lakes in the Canadian High Arctic [*Jackson et al*., 2004; *Jackson*, 2015]. While these sediments show increasing THg accumulation in lakes since the nineteenth century, there are indications that at least some of the Hg isotopic variations recorded in the sediments may be driven by in situ fractionation effects linked to microbial activity and/or derived from terrigeneous inputs from the watershed [*Jackson*, 2015; *Chen et al*., 2016], which hampers comparison with our firn and ice core data. However, our data could assist in constraining the possible sources of Hg isotopic variability observed in Arctic lake sediment records.

Glacier firn, like lake sediments, is a dynamic medium that can be transformed by ambient environmental conditions. For example, stratigraphic analysis of firn cores from the Canadian Arctic have revealed increasing rates of surface summer melt in the late 20th and early 21st centuries [*Fisher et al*., 2012]. These rising melt rates are accompanied by downward percolation and refreezing of meltwater in the firn. On Agassiz ice cap and on the Prince of Wales icefield, these changes began in the 1980s and so far have primarily affected the stratigraphy of shallow firn layers. However, the possible impact of meltwater percolation on Hg isotopic variations recorded in polar firn cores is presently unknown and should be investigated in order to better constrain the interpretation of data from these cores.

Acknowledgments
The complete data for this paper are available in supporting information Tables S1–S7. SEM-EDX analyses of particles in the DV99.1 core (Figure S1) were performed by Glenn Poirier at the University of Ottawa-Canadian Museum of Nature MicroAnalysis Laboratory. This project was supported by a grant from the Northern Contaminants Program (Indigenous and Northern Affairs Canada), by an Industrial Fellowship from Canada's National Science and Engineering Research Council (NSERC) to E. Krümmel from 2009 to 2011, and by an NSERC Discovery grant to A. Poulain. M. Štrok and J. Chen also acknowledge support by the Ontario Ministry of Research & Innovation Post-Doctoral Fellowship program. J. Chen was further financially supported by the Natural Science Foundation of China (41273023 and U1301231), National "973" Program (2013CB430001), and Strategic Priority Research Program (XDB05030302). We are thankful for comments by two anonymous reviewers which helped to improve this manuscript.

References

Amos, H. M., D. J. Jacob, D. G. Streets, and E. M. Sutherland (2013), Legacy impacts of all-time anthropogenic emissions on the global mercury cycle, *Global Biogeochem. Cycles*, *27*, 1–12, doi:10.1002/gbc.20040.

Arctic Monitoring and Assessment Programme (2011), *AMAP Assessment 2011: Mercury in the Arctic*, 193 pp., AMAR, Oslo.

Barker, J. D., M. J. Sharp, S. J. Fitzsimons, and R. J. Turner (2006), Abundance and dynamics of dissolved organic carbon in glacier systems, *Arctic. Antarct. Alp. Res.*, *38*, 163–172.

Bartels-Rausch, T., T. Huthwelker, M. Jöri, H. Gäggeler, and M. Ammann (2008), Interaction of gaseous elemental mercury with snow surfaces: Laboratory investigation, *Environ. Res. Lett.*, *3*, 04500, doi:10.1088/1748-9326/3/4/045009.

Beal, S. A., E. C. Osterberg, C. M. Zdanowicz, and D. A. Fisher (2015), An ice core perspective on mercury pollution during the past 600 years, *Environ. Sci. Technol.*, *49*, 7641–7647.

Berger, A. (1992), Orbital variations and insolation database. IGBP PAGES/World Data Center for Paleoclimatology.

Bergquist, B. A., and J. D. Blum (2007), Mass-dependent and mass-independent fractionation of Hg isotopes by photoreduction in aquatic systems, *Science*, *318*, 417–420.

Blum, J. D., and B. A. Bergquist (2007), Reporting the variations in the natural isotopic composition of mercury, *Anal. Bioanal. Chem.*, *388*, 353–359.

Blum, J. D., L. S. Sherman, and M. W. Johnson (2014), Mercury isotopes in Earth and environmental sciences, *Annu. Rev. Earth Planrt. Sci.*, *42*, 249–269.

Briner, J. P., et al. (2016), Holocene climate change in Arctic Canada and Greenland, *Quat. Sci. Rev.*, doi:10.1016/j.quascirev.2016.02.010.

Cai, H., and J. Chen (2016), Mass-independent fractionation of even mercury isotopes, *Chinese Sci. Bull.*, *61*, 116–124.

Cai, Y., R. Jaffe, A. Alli, and R. D. Jones (1996), Determination of organomercury compounds in aqueous samples by capillary gas chromatography-atomic fluorescence spectrometry following solid-phase extraction, *Anal. Chim. Acta*, *334*, 251–259.

Chen, J., H. Hintelmann, and B. Dimock (2010), Chromatographic pre-concentration of Hg from dilute aqueous solutions for isotopic measurement by MC-ICP-MS, *J. Anal. Atom. Spectrom.*, *25*, 1402–1409.

Chen, J., H. Hintelmann, X.-B. Feng, and B. Dimock (2012), Unusual fractionation of both odd and even mercury isotopes in precipitation from Peterborough, ON, Canada, *Geochim. Cosmochim. Acta*, *90*, 33–46.

Chen, J., H. Hintelmann, W. Zheng, X. Feng, H. Cai, Z. Wang, S. Yuan, and Z. Wang (2016), Isotopic evidence for distinct sources of mercury in lake waters and sediments, *Chem. Geol.*, *426*, 33–44.

Craig, H., Y. Horibe, and T. Sowers (1988), Gravitational separation of gases and isotopes in polar ice caps, *Science*, *242*, 1675–1678.

Demers, J. D., J. D. Blum, and D. R. Zak (2013), Mercury isotopes in a forested ecosystem: Implications for air-surface exchange dynamics and the global mercury cycle, *Global Biogeochem. Cycles*, *27*, 222–238, doi:10.1002/gbc.20021.

Demers, J. D., L. S. Sherman, J. D. Blum, F. J. Marsik, and J. T. Dvonch (2015), Coupling atmospheric mercury isotope ratios and meteorology to identify sources of mercury impacting a coastal urban-industrial region near Pensacola, Florida, USA, *Global Biogeochem. Cycles*, *29*, 1689–1705, doi:10.1002/2015GB005146.

Driscoll, C. T., R. P. Mason, H. M. Chan, D. J. Jacob and N. Pirrone (2013), Mercury as a global pollutant: Sources, pathways, and effects. *Environ. Sci. Technol.*, *47*, 4967−4983.

Durnford, D., and A. Dastoor (2011), The behavior of mercury in the cryosphere: A review of what we know from observations, *J. Geophys. Res.*, *116*, D06305, doi:10.1029/2010JD014809.

Durnford, D., A. Dastoor, D. Figueras-Nieto, and A. Ryjkov (2010), Long range transport of mercury to the Arctic and across Canada, *Atmos. Chem. Phys.*, *10*, 6063–6086.

Engström, D. R., W. F. Fitzgerald, C. A. Cooke, C. H. Lamborg, P. E. Drevnick, E. B. Swain, S. J. Balogh and P. H. Balcom (2014), Atmospheric Hg emissions from preindustrial gold and silver extraction in the Americas: A re-evaluation from lake-sediment archives. *Environ. Sci. Technol.*, *48*, 6533−6543.

Estrade, N., J. Carignan, and O. F. X. Donard (2011), Tracing and quantifying anthropogenic mercury sources in soils of northern France using isotopic signatures, *Environ. Sci. Technol.*, *45*, 1235–1242.

Faïn, X., C. P. Ferrari, A. Dommergue, A. Albert, M. Battle, L. Arnaud, J. M. Barnola, W. Cairns, C. Barbante, and C. Boutron (2008), Mercury in the snow and firn at Summit Station, Central Greenland, and implications for the study of past atmospheric mercury levels, *Atmos. Chem. Phys.*, *8*, 3441–3457.

Ferrari, C. P., A. Dommergue, C. F. Boutron, H. Skov, M. Goodsite, and B. Jensen (2004), Nighttime production of elemental gaseous mercury in interstitial air of snow at Station Nord, Greenland, *Atmos. Environ.*, *38*, 2727–2735.

Fisher, D. A., R. M. Koerner, and N. Reeh (1995), Holocene climatic records from Agassiz ice cap, Ellesmere Island, NWT, Canada, *Holocene*, *5*, 19–24.

Fisher, D. A., et al. (1998), Penny Ice Cap cores, Baffin Island, Canada, and the Wisconsinan Foxe Dome connection: Two states of Hudson Bay ice cover, *Science*, *279*, 692–695.

Fisher, D. A., J. Zheng, D. Burgess, C. Zdanowicz, C. Kinnard, M. Sharp, and J. Bourgeois (2012), Recent melt rates of Canadian Arctic ice caps are the highest in four millennia, *Global Planet. Change*, *84–85*, 3–7.

Fitzgerald, W. F., D. R. Engstrom, R. P. Mason, and E. A. Nater (1998), The case for atmospheric mercury contamination in remote areas, *Environ. Sci. Technol.*, *32*, 1–7.

Gamberg, M., J. Chételat, A. Poulain, C. Zdanowicz, and J. Zheng (2015), Mercury in the Canadian Arctic terrestrial environment: An update, *Sci. Total Environ.*, *509–510*, 28–40.

Goodsite, M. E., P. M. Outridge, J. H. Christensen, A. Dastoor, D. Muir, O. Travnikov, and S. Wilson (2013), How well do environmental archives of atmospheric mercury deposition in the Arctic reproduce rates and trends depicted by atmospheric models and measurements? *Sci. Total Environ.*, *452–453*, 196–207.

Goto-Azuma, K., and R. M. Koerner (2001), Ice core studies of anthropogenic sulfate and nitrate trends in the Arctic, *J. Geophys. Res.*, *206*, 4959–4969, doi:10.1029/2000JD900635.

Gratz, L. E., G. J. Keeler, J. D. Blum, and L. S. Sherman (2010), Isotopic composition and fractionation of mercury in Great Lakes precipitation and ambient air, *Environ. Sci. Technol.*, *44*, 7764–7770.

Gray, J. E., M. J. Pribil, P. C. Van Metre, D. M. Borrok, and A. Thapalia (2013), Identification of contamination in a lake sediment core using Hg and Pb isotopic compositions, Lake Ballinger, Washington, USA, *Appl. Geochem.*, *29*, 1–12.

Horowitz, H. M., D. J. Jacob, H. M. Amos, D. G. Streets, and E. M. Sunderland (2014), Historical mercury releases from commercial products: Global environmental implications. *Environ. Sci. Technol.*, *48*, 10,242−10,250.

Jackson, T. A. (2015), Evidence for mass-independent fractionation of mercury isotopes by microbial activities linked to geographically and temporally varying climatic conditions in Arctic and subarctic lakes, *Geomicrobiol. J.*, *32*, 799–826.

Jackson, T. A., D. C. G. Muir, and W. Vincent (2004), Historical variations in the stable isotope composition of mercury in Arctic lake sediments, *Environ. Sci. Technol.*, *38*, 2813–2821.

Jiskra, M., J. G. Wiederhold, B. Bourdon, and R. Kretzschmar (2012), Solution speciation controls mercury isotope fractionation of Hg(II) sorption to goethite, *Environ. Sci. Technol.*, *46*, 6654–6662.

Kinnard, C., C. Zdanowicz, D. Fisher, and C. Wake (2006), Calibration of an ice-core glaciochemical (sea salt) record with sea ice variability in the Canadian Arctic, *Ann. Glaciol.*, *44*, 383–390.

Kinnard, C., R. Koerner, C. Zdanowicz, J. Zheng, M. Sharp, L. Nicholson, and B. Lauriol (2008), Stratigraphic analysis of an ice core from the Prince of Wales icefield, Ellesemere Island, Arctic Canada, using digital image analysis, *J. Geophys. Res.*, *113*, D24120, doi:10.1029/2008JD011083.

Koerner, R. M. (1979), Accumulation, ablation, and oxygen isotope variations on the Queen Elizabeth Islands ice caps, Canada, *J. Glaciol.*, *22*, 25–41.

Kuhn, T., R. Damoah, A. Bacak, and J. J. Sloan (2010), Characterizing aerosol transport into the Canadian High Arctic using aerosol mass spectrometry and Lagrangian modelling, *Atmos. Chem. Phys.*, *10*, 10,489–10,502.

Ma, J., H. Hintelmann, J. L. Kirk, and D. C. G. Muir (2013), Mercury concentrations and mercury isotope composition in lake sediment cores from the vicinity of a metal smelting facility in Flin Flon, Manitoba, *Chem. Geol.*, *336*, 96–102.

Mann, E., S. Ziegler, M. Mallory, and N. O'Driscoll (2014), Mercury photochemistry in snow and implications for Arctic ecosystems, *Environ. Rev.*, *22*, 331–345.

O'Concubhair, R., D. O'Sullivan, and J. R. Sodeau (2012), Dark oxidation of dissolved gaseous mercury in polar ice mimics, *Environ. Sci. Technol.*, *46*, 4829–4836.

Okuyama, J., H. Narita, T. Hondoh and R. M. Koerner (2003), Physical properties of the P96 ice core from Penny Ice Cap, Baffin Island, Canada, and derived climatic records. *J. Geophys. Res.*, *108*(B2), 2090, doi:10.1029/2001JB001707.

Poulain, A., J. D. Lalonde, M. Amyot, J. A. Shead, F. Roafie, and P. A. Ariya (2004), Redox transformations of mercury in an Arctic snowpack at springtime, *Atmos. Environ.*, *38*, 6763–6774.

Poulain, A., E. Garcia, M. Amyot, P. G. C. Campbell, and P. A. Ariya (2007), Mercury distribution, partitioning and speciation in coastal vs. inland High Arctic snow, *Geochim. Cosmochim. Acta*, *71*, 3419–3431.

Rose, C. H., S. Ghosh, J. D. Blum, and B. A. Bergquist (2015), Effects of ultraviolet radiation on mercury isotope fractionation during photo-reduction for inorganic and organic mercury species, *Chem. Geol.*, *405*, 102–111.

Schroeder, W. H., K. G. Anlauf, L. A. Barrie, J. Y. Lu, A. Steffen, D. R. Schneeberger, and T. Berg (1998), Arctic springtime depletion of mercury, *Nature*, *394*, 331–332.

Schuster, P. F., D. P. Krabbenhoft, D. L. Naftz, L. D. Cecil, M. L. Olson, J. F. Dewild, D. D. Susong, J. R. Green and M. L. Abbott (2002), Atmospheric mercury deposition during the last 270 years: A glacial ice core record of natural and anthropogenic sources. *Environ. Sci. Technol.*, *36*, 2303−2310.

Severinghaus, J. P., A. Grachev, and M. Battle (2001), Thermal fractionation of air in polar firn by seasonal temperature gradients, *Geochem. Geophys Geosyst.*, *2*, 1048, doi:10.1029/2000GC000146.

Sherman, L. S., J. D. Blum, K. P. Johnson, G. J. Keeler, J. A. Barres, and T. A. Douglas (2010), Mass-independent fractionation of mercury isotopes in Arctic snow driven by sunlight, *Nat. Geosci.*, *3*, 173–177.

Sherman, L. S., J. D. Blum, J. D. Douglas, and A. Steffen (2012a), Frost flowers growing in the Arctic ocean-atmosphere–sea ice–snow interface: 2. Mercury exchange between the atmosphere, snow, and frost flowers, *J. Geophys. Res.*, *117*, D00R10, doi:10.1029/2011JD016186.

Sherman, L. S., J. D. Blum, G. J. Keeler, J. D. Demers, and J. T. Dvonch (2012b), Investigation of local mercury deposition from a coal-fired power plant using mercury isotopes, *Environ. Sci. Technol.*, *46*, 382–390.

Sherman, L. S., J. D. Blum, T. Dvonch, L. E. Gratz, and M. S. Landis (2015), The use of Pb, Sr, and Hg isotopes in Great Lakes precipitation as a tool for pollution source attribution, *Sci. Total Environ.*, *502*, 362–374.

Simpson, W. R., et al. (2007), Halogens and their role in polar boundary-layer ozone depletion, *Atmos. Chem. Phys.*, *7*, 4375–4418.

Smith, R. S., J. G. Wiederhold, A. D. Jew, G. E. Brown Jr., B. Bourdon, and R. Kretzschmar (2014), Small-scale studies of roasted ore waste reveal extreme ranges of stable mercury isotope signatures, *Geochim. Cosmochim. Acta*, *137*, 1–17.

Søndergaard, J., M. Tamstorf, B. Elberling, M. M. Larsena, M. Rask Mylius, M. Lund, J. Abermann, and F. Rigét (2015), Mercury exports from a High-Arctic river basin in northeast Greenland (74°N) largely controlled by glacial lake outburst floods, *Sci. Total Environ.*, *514*, 83–91.

Sonke, J. E. (2011), A global model of mass independent mercury stable isotope fractionation, *Geochim. Cosmochim. Acta*, *75*, 4577–4590.

Sonke, J. E., J. Schäfer, J. Chmeleff, S. Audry, G. Blanc, and B. Dupré (2010), Sedimentary mercury stable isotope records of atmospheric and riverine pollution from two major European heavy metal refineries, *Chem. Geol.*, *279*, 90–100.

St. Louis, V. L., H. Hintelmann, J. A. Graydon, J. L. Kirk, J. Barker, B. Dimock, M. J. Sharp, and I. Lehnherr (2007), Methylated mercury species in Canadian high Arctic marine surface waters and snowpacks, *Environ. Sci. Technol.*, *41*(18), 6433–6441.

St. Louis, V., M. Sharp, A. Steffen, A. May, J. Barker, J. Kirk, D. Kelly, S. Arnott, B. Keatley, and J. Smol (2005), Some sources and sinks of monomethyl and inorganic mercury on Ellesmere Island in the Canadian High Arctic, *Environ. Sci. Technol.*, *39*, 2686–2701.

St. Pierre, K. A., V. C. St. Louis, J. L. Kirk, I. Lenherr, S. Wang, and C. La Farge (2015), Importance of open marine waters to the enrichment of total mercury and mono-methylmercury in lichens in the Canadian High Arctic, *Environ. Sci. Technol.*, *49*, 5930–5938.

Steffen, A., et al. (2008), A synthesis of atmospheric mercury depletion event chemistry linking atmosphere, snow and water, *Atmos. Chem. Phys.*, *8*, 1445–1482.

Steffen, A., I. Lehnherr, A. Cole, P. Ariya, A. Dastoor, D. Durnford, J. Kirk, and M. Pilote (2015), Atmospheric mercury in the Canadian Arctic. Part I: A review of recent field measurements, *Sci. Total Environ.*, *509–510*, 3–15.

Stetson, S. J., J. E. Gray, R. B. Wanty, and D. Macalady (2009), Isotopic variability of mercury in ore, mine-waste calcine, and leachates of mine-waste calcine from areas mined for mercury, *Environ. Sci. Technol.*, *43*, 7331–7336.

Stibal, M., E. C. Lawson, G. P. Lis, K. M. Mak, J. L. Wadham, and A. M. Anesio (2010), Organic matter content and quality in supraglacial debris across the ablation zone of the Greenland ice sheet, *Ann. Glaciol.*, *51*, 1–8.

Streets, D. G., M. K. Devane, Z. Lu, T. C. Bond, E. M. Sunderland, and D. J. Jacob (2011), All-time releases of mercury to the atmosphere from human activities, *Environ. Sci. Technol.*, *45*, 10,485–10,491.

Štrok, M., H. Hintelmann, and B. Dimock (2014), Development of pre-concentration procedure for the determination of Hg isotope ratios in seawater samples, *Anal. Chim. Acta*, *851*, 57–63.

Štrok, M., P. A. Baya, and H. Hintelmann (2015), The mercury isotope composition of Arctic coastal seawater, *C. R. Geosci.*, *347*, 368–376.

Sun, R., J. E. Sonke, L.-E. Heimb-rger, H. E. Belkin, G. Liu, D. Shome, E. Cukrowska, C. Liousse, O. S. Pokrovsky, and D. G. Streets (2014), Mercury stable isotope signatures of world coal deposits and historical coal combustion emissions. *Environ. Sci. Technol.*, *48*, 7660−7668.

Sun, R., D. G. Streets, H. M. Horowitz, H. M. Amos, G. Liu, V. Perrot, J.-P. Toutain, H. Hintelmann, E. Sunderland, and J. E. Sonke (2016), Historical (1850–2016) mercury stable isotope inventory from athropogenic sources to the atmosphere, *Elementa*, *4*, doi:10.12952/journal.elementa.000091.

U.S. Environmental Protection Agency (2002), US-EPA Method 1631, Revision E: Mercury in water by oxidation, purge and trap, and cold vapor atomic fluorescence spectrometry. EPA-821-R-02-019. US-EPA, Washington, 38 p.

United Nations Environment Programme (2013), *Minamata Convention on Mercury: Text and Annexes*, 63 pp., UNEP, Geneva.

Vinther, B. M., H. B. Clausen, D. A. Fisher, R. M. Koerner, S. J. Johnsen, K. K. Andersen, D. Dahl-Jensen, S. O. Rasmussen, J. P. Steffensen, and A. M. Svensson (2008), Synchronizing ice cores from the Renland and Agassiz ice caps to the Greenland ice core chronology, *J. Geophys. Res.*, *113*, D08115, doi:10.1029/2007JD009143.

Walker, M. J. C., M. Berkelhammer, L. C. Cwynar, D. A. Fisher, A. J. Long, J. J. Lowe, R. M. Newnham, S. O. Rasmussen, and H. Weiss (2012), Formal subdivision of the Holocene Series/Epoch: A discussion paper by a working group of INTIMATE (Integration of Ice-Core, Marine and Terrestrial Records) and the Subcommission on Quaternary Stratigraphy (International Commission on Stratigraphy), *J. Quat. Sci.*, *27*, 649–659.

Wang, Z., J. Chen, X. Feng, H. Hintelmann, S. Yuan, H. Cai, Q. Huang, S. Wang and F. Wang (2015), Mass-dependent and mass-independent fractionation of mercury isotopes in precipitation from Guiyang, SW China. *C. R. Geosci.*, *347*, 358−367.

Wiederhold, J. G., R. S. Smith, H. Siebner, A. D. Jew, G. E. Brown Jr., B. Bourdon, and R. Kretzschmar (2013), Mercury isotope signatures as tracers for Hg cycling at the New Idria Hg mine. *Environ. Sci. Technol.*, *47*, 6137−6145.

Yin, R., X. Feng, and W. Shi (2010), Application of the stable-isotope system to the study of sources and fate of Hg in the environment: A review, *Appl. Geochem.*, *25*, 1467–1477.

10.1002/2016GB005411

Yin, R., X. Feng, J. Wang, P. Li, J. Liu, Y. Zhang, J. Chen, L. Zheng, and T. Hu (2013), Mercury speciation and mercury isotope fractionation during ore roasting process and their implication to source identification of downstream sediment in the Wanshan mercury mining area, SW China, *Chem. Geol.*, *336*, 72–79.

Zambardi, T., J. E. Sonke, J. P. Toutain, F. Sortino, and H. Shinohara (2009), Mercury emissions and stable isotopic compositions at Vulcano Island (Italy), *Earth Planet. Sci. Lett.*, *277*, 236–243.

Zdanowicz, C., E. Krümmel, D. Lean, A. Poulain, E. Yumvihoze, J. Chen, and H. Hintelmann (2013), Accumulation, storage and release of atmospheric mercury in a glaciated Arctic catchment, Baffin Island, Canada, *Geochim. Cosmochim. Acta*, *107*, 316–335.

Zdanowicz, C., E. M. Kruemmel, D. Lean, A. Poulain, C. Kinnard, E. Yumvihoze, J. Chen, and H. Hintelmann (2015), Pre-industrial and recent (1970–2010) atmospheric deposition of sulfate and mercury in snow on southern Baffin Island, Canada, *Sci. Total Environ.*, *509–510*, 104–114.

Zhang, Y., L. Jaeglé, L. Thompson, and D. G. Streets (2014), Six centuries of changing oceanic mercury, *Global Biogeochem. Cycles*, *28*, 1251–1261, doi:10.1002/2014GB004939.

Zheng, J. (2014), Archives of total mercury reconstructed with ice and snow from Greenland and the Canadian High Arctic, *Sci. Total Environ.*, *509–510*, 133–144.

Zheng, J., D. Fisher, E. Blake, G. Hall, J. Vaive, M. Krachler, C. Zdanowicz, J. Lam, G. Lawson, and W. Shotyk (2006), An ultra-clean firn core from Devon Ice Cap, Nunavut, Canada, retrieved using a specially-designed titanium drill for trace element studies, *J. Environ. Monit.*, *8*, 406–413.

Zheng, J., P. Pelchat, J. Vaive, D. Bass, and F. Ke (2014), Total mercury in snow and ice samples from Canadian High Arctic ice caps and glaciers: A practical procedure and method for total Hg quantification at low pg g^{-1} level, *Sci. Total Environ.*, *468–469*, 487–494.